Zeitschrift: Schweizerische mineralogische und petrographische Mitteilungen = Bulletin suisse de minéralogie et pétrographie

Band: 84 (2004)

Heft: 1-2: Geodynamics and Ore Deposit Evolution of the Alpine-Carpathian-Balkan-Dinaride Orogenic System

Artikel: Variscan to Alpine tectonothermal evolution of the Central Srednogorie unit, Bulgaria: constraints from 40Ar/39Ar analysis

Autor: Velichkova, Svetlana H. / Handler, Robert / Neubauer, Franz

DOI: https://doi.org/10.5169/seals-63743

Schweizerische Mineralogische und Petrographische Mitteilungen 84, 133–151, 2004

Variscan to Alpine tectonothermal evolution of the Central Srednogorie unit, Bulgaria: constraints from $^{40}Ar/^{39}Ar$ analysis

Svetlana H. Velichkova [1,2], *Robert Handler* [1], *Franz Neubauer* [1] and *Zivko Ivanov* [2]

Abstract

The Panagyurishte region, east of Sofia in Bulgaria, is characterised by amphibolite facies metamorphic basement rocks, overlain by Late Carboniferous to Triassic and Late Cretaceous cover sequences, which together comprise the Central Part of the Srednogorie unit. This succession is intruded by subvolcanic Cretaceous calcalkaline magmatic bodies, which are part of the so-called Banatite Belt and host world-class Cu–Au-deposits. The goal of this study is to constrain the age of tectonometamorphic events recorded in the Srednogorie basement.

The amphibolite facies metamorphic Srednogorie basement consists of two-mica gneisses, micaschists, orthoamphibolites, small serpentinite bodies, and anatexites of pre-Upper Carboniferous age. New $^{40}Ar/^{39}Ar$ ages of white mica and biotite from southern and northern sectors of the central part of the Srednogorie unit show well-defined Late Palaeozoic plateau ages of ca. 317–305 Ma, which indicate a Variscan age for the postmetamorphic cooling after the last amphibolite facies metamorphic overprint. Subsequent post-Variscan intrusion and slow cooling of the cross-cutting Poibrene diorite is indicated by Late Palaeozoic cooling ages of 302.9 ± 1.4 and 263.00 ± 0.69 Ma reported for hornblende and biotite, respectively.

During the Cretaceous, southern sectors of the Srednogorie basement and overlying Late Carboniferous to Triassic cover successions were affected by greenschist facies metamorphic overprint. The latter event is limited to southern sectors near Alpine low-angle normal faults. Muscovite and biotite samples from several subhorizontal ductile shear zones yield consistent Cretaceous $^{40}Ar/^{39}Ar$ plateau ages of ca. 99–105 Ma. Greenschist facies retrogression affected the basement mainly along basement-cover (Stefanian-Permian) contacts, which are strongly sheared. Subsequently, the steep ductile dextral Maritsa shear zone formed along a belt of granitoid intrusions within rheologically weakened crust along southern margins of the Panagyurishte region, whereas the Central Srednogorie collapse-type basin seals structures formed during early Late Cretaceous.

Keywords: Variscan orogeny, retrogression, ductile shear zone, extension, polymetamorphism.

Introduction

Large parts of internal sectors of the Alpine-Balkan-Carpathian-Dinaride (ABCD) orogen (Fig. 1) have been affected by Cretaceous tectonic events, often referred to represent the "Austrian" phase of deformation, mostly recorded in sedimentary sections by pronounced angular unconformities and breaks in sedimentation (e.g. Foose and Manheim, 1975; Hsü et al., 1977; Ivanov et al., 1979; Burchfiel, 1980; Ivanov, 1983, 1988; Nachev, 1993; Channell and Kozur, 1997; Stampfli and Mosar, 1999; Neugebauer et al., 2001). During the last decade much evidence arose that deformation in pre-Cretaceous high-grade metamorphic continental basement rocks resulted in Cretaceous ductile shearing causing localised or pervasive retrogression. A closer look shows that deformation occurred in two stages: (1) an earlier stage of thick-skinned tectonic thrusting and formation of an orogenic wedge and (2) a subsequent stage of extension associated with late-stage orogenic collapse (e. g. Neubauer et al., 1995; Dallmeyer et al., 1996; Willingshofer et al., 1999). Retrogression in pre-Alpine basement rocks from the ABCD orogen has been dated by the $^{40}Ar/^{39}Ar$ method to have occurred between ca. 120 and 78 Ma. Thereby an older age group (ca. 120 to 90 Ma) always is related to thrusting (e. g. Dallmeyer et al., 1996). A younger age group (mostly between 90 and 78 Ma) is often related to extensional collapse, which was associated with the formation of sedimentary basins (often referred to as "Gosau" after a type of basin in the Eastern Alps) and the formation of ductile low-angle normal faults at middle crustal levels) and contemporaneous shortening in deep crustal levels (e. g., Willingshofer et al., 1999; Liu et al., 2001). Basin formation largely occurred

[1] Institute of Geology and Palaeontology, University of Salzburg, Hellbrunner Str. 34, A-5020 Salzburg, Austria. e-mail:<robert.handler@sbg.ac.at>, <franz.neubauer@sbg.ac.at>
[2] Dept. of Geology, Sofia University, Sofia, Tzar Osvoboditel Blv. 15, Sofia 1000, Bulgaria.

0036-7699/04/0084/133

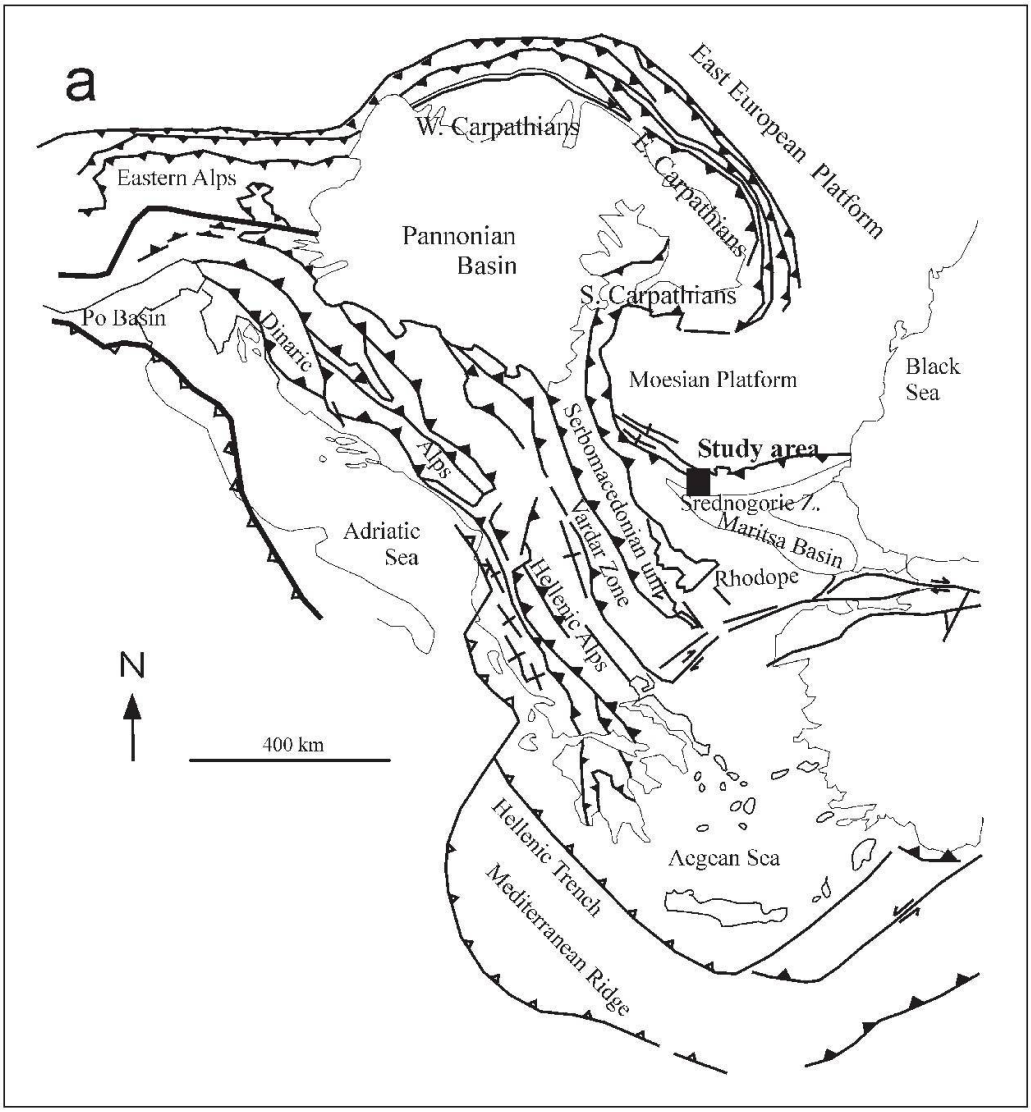

Fig. 1 (a) Geological overview map of the Alpine-Carpathian-Dinaride-Balkan orogenic belt (modified after Royden, 1988). (b) Map of the Balkan, Rhodopian and Serbomacedonian units (modified after Haydoutov et al., 1997).

during late orogenic stages in a compressional regime with orogen-parallel extension (e. g. Neubauer et al., 1995; Willingshofer et al., 1999).

Another issue concerning the internal sectors of the ABCD orogen is the nature and age of the pre-Mesozoic continental basement. More and more evidence arises that the basement includes two distinct major high-grade metamorphic complexes: (1) a Cadomian-age basement, which is only partly overprinted by Variscan tectonic events (e. g., Neubauer 2002b and references therein) and (2) a high-grade metamorphic, often migmatitic basement complex of undisputed Variscan age (e. g. Dallmeyer et al., 1996, 1998).

These issues have not yet been fully examined in the Balkan area by modern geochronological methods. Here we present new $^{40}Ar/^{39}Ar$ mineral ages from the basement of the Srednogorie unit with the main emphasis to constrain the age of the last pervasive tectonothermal overprint and/or the age of more localised retrogression. The data may help to constrain models of the tectonic evolution in the region, which hosts significant late Cretaceous massive sulphide and porphyry Cu-type ores (e. g. Popov and Popov, 2000; Heinrich and Neubauer, 2002 and references therein). The tectonic evolution seems to be largely similar to that of the rest of the internal Alpine-Balkan-Carpathian-Dinaride region, with Gosau-type collapse basins, containing abundant shallow-level plutonic and volcanic rocks in their basin fill (Neubauer, 2002a and references therein).

Geological setting

The Balkan/Rhodope region comprises a number of tectonic units, which are from north to south: the Fore-Balkan unit, which is southerly adjacent to the Moesian platform, the Balkan unit, the Srednogorie unit, the Rhodopian unit, and the Serbomacedonian unit (Fig. 1b). The Fore-Balkan, Balkan and Srednogorie units are considered

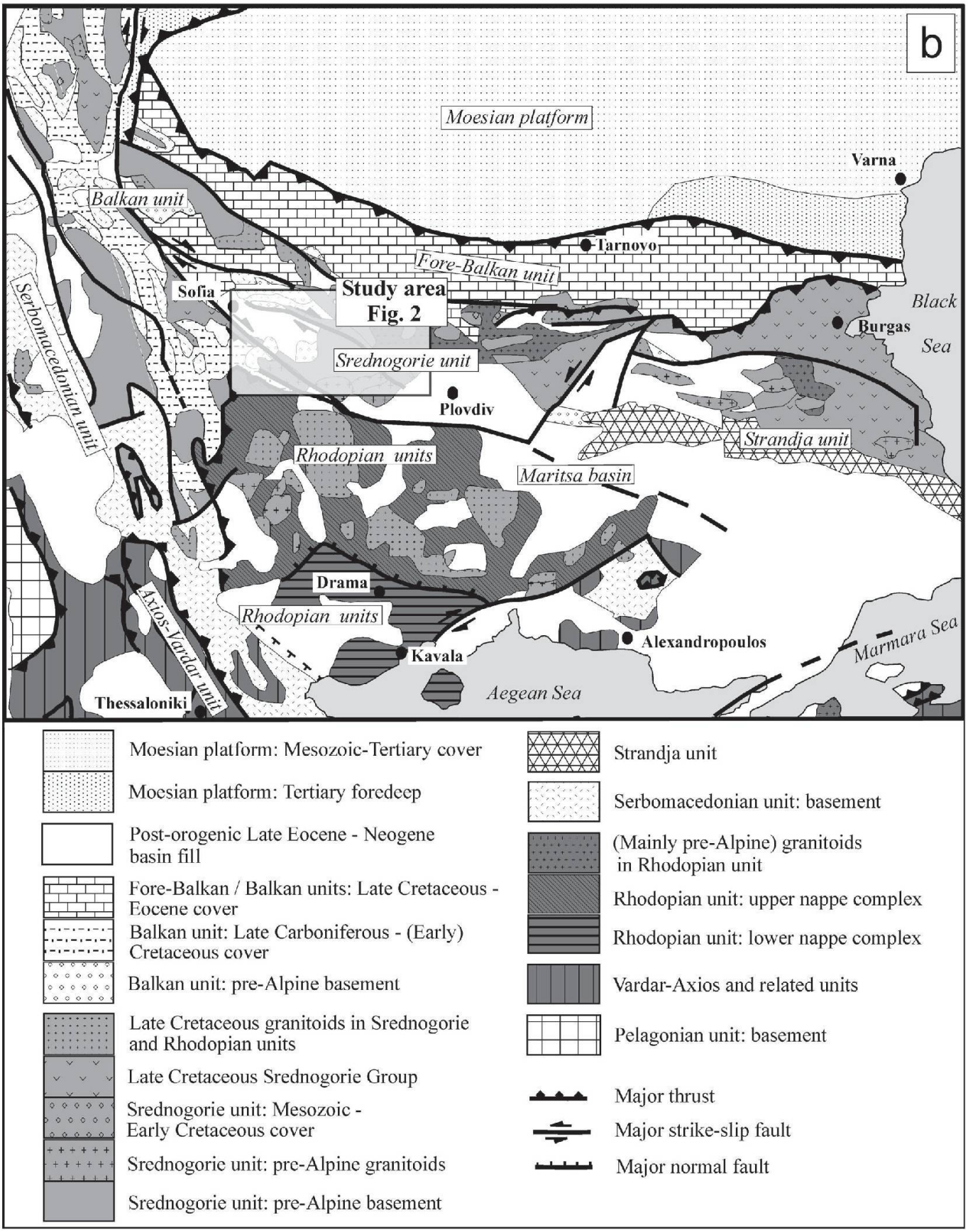

Fig. 1b

to represent zones with a metamorphic, continental basement and cover successions comprising Late Carboniferous to Eocene strata (Fig. 2). The basement is locally termed as Balkanide type (Ivanov, 1989a,b, 2002) or Balkan terrane (Haydoutov and Yanev, 1997) and includes migmatitic orthogneisses, some paragneisses and amphibolites.

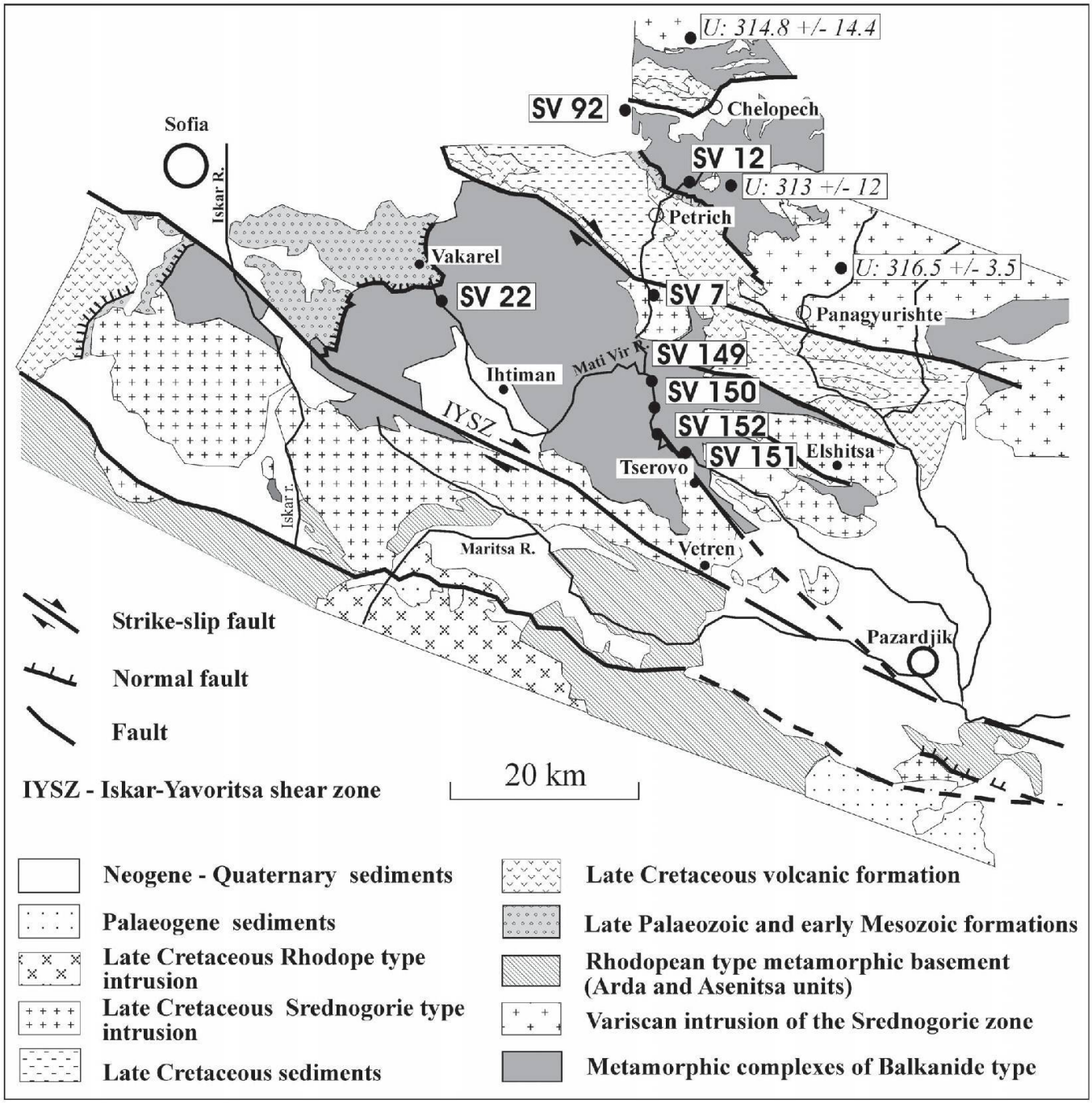

Fig. 2 Simplified tectonic map of the Central Srednogorie and northern Rhodope zones and locations of studied samples.

The amphibolite facies metamorphic basement consists of two-mica orthogneisses, micaschists, orthoamphibolites, small serpentinite bodies, and anatexites. The typical metamorphic mineral assemblage of the amphibolite facies metapelites is Pl + Bt + Sill + Gr, and Kfs + Bt + Gr for the migmatites (Dimitrova and Belmustakova, 1982). The age of the basement rocks was believed to be Proterozoic (Dimitrov, 1959) or Archaen (Kozhukharov et al., 1978). Ivanov (1989a, b) inferred a Palaeozoic age ("Balkanide-type" metamorphic complex in his terminology) on the basis of its field relations with the overlying Upper Carboniferous–Permian conglomerates.

U–Pb ages obtained on zircons from these basement gneisses are 406 ± 30, 480 ± 30 and 485 ± 50 Ma (Arnaudov et al., 1989). Recent U–Pb zircon data from the post-metamorphic Vezhen granite gave an age of 314.8 ± 14.4 Ma (Kamenov et al., 2002). Peytcheva and von Quadt (2003) reported inherited zircons with an age of 442.7 ± 8.3 Ma from the Velichkovo gabbro.

The cover successions of the Srednogorie unit comprise Late Carboniferous to Lower Triassic clastic sequences, Middle Triassic limestone and Upper Triassic sandstones, followed by Jurassic and Lower Cretaceous carbonatic successions (Foose and Manheim, 1975; Minkovska et al.,

2002). Late Early Cretaceous tectonism ("Austrian phase") characterised by thrusting and folding is associated with a weak, southward increasing metamorphism, which affected basement and cover (e. g. Karagjuleva et al., 1974). The metamorphic overprint occurred under very low- to low-grade metamorphic conditions, based on the overprint of the Mesozoic successions. Deformation and metamorphism are interpreted to relate with closure and collision of the Vardar-Axios oceanic belt with the continental Serbomacedonian block (Ricou et al., 1998). Subsequent post-contractional basins formed constituting together the Srednogorie Group, the volcanosedimentary infill of these basins. Clastic sedimentary rocks are associated with calc-alkaline and subordinate alkaline volcanic and plutonic rocks belonging to the Srednogorie unit. These magmatic rocks are partly rich in ore mineralisation (Aiello et al., 1977; Berza et al., 1998; Boccaletti et al., 1974, 1978; Popov and Popov, 2000). The basin fill comprises clastic successions, such as terrestrial and marine, turbiditic conglomerates, and sandstones, which are intercalated by marls, shales, and tuffs. The stratigraphic range of the volcano-sedimentary complex is Coniacian to Campanian (Aiello et al., 1977; Popov and Popov, 2000).

The dextral, oblique-slip Late Cretaceous/Tertiary Maritsa fault separates the Srednogorie unit from the southerly adjacent Rhodopian metamorphic complex to the south (Ivanov et al., 2001b). The Iskar-Yavoritsa shear zone is part of the Maritsa fault and represents a late Cretaceous dextral transtensional shear zone with relative upwards motion of the Rhodopian metamorphic complex and subsidence of the Srednogorie basin (Ivanov, 1989b; Burg et al., 1990, 1993; Ivanov et al., 2001b). The Iskar-Yavoritsa shear zone is intruded by Upper Cretaceous granites and diorites, which are partly affected by ductile shearing (Ivanov et al., 2001b). The age of intrusions varies between 84 and 78 Ma (Kamenov et al., 2002; Peytcheva and von Quadt, 2003). Therefore, the time span represents the minimum duration of shearing.

The Rhodopian metamorphic complex extends from Bulgaria to Greece and westernmost Turkey. It comprises a stack of metamorphic nappes, which are younging in age of metamorphism towards the footwall (Burg et al., 1990; Zagorcev, 1993; Ricou et al., 1998; Krohe and Mposkos, 2002). The metamorphic ages range from ca. 120 Ma in the hangingwall units to ca. 35 Ma in the lowermost unit (Krohe and Mposkos, 2002 and references therein). This suggests a continuous accretion of metamorphic units towards the footwall in the south. Barr et al. (1999) considered the Rhodopian metamorphic complex as representing an accretionary wedge, which formed within a N-dipping subduction zone (Ricou et al., 1998). Due to the younging of metamorphism from late Early Cretaceous (uppermost units) to Oligocene ages (lowermost unit), continuous or stepwise exhumation of metamorphic complexes is partly contemporaneous with the Late Cretaceous subsidence in the Srednogorie basin. This matches the observation of a southerly located hinterland of clastic successions in the Srednogorie basin (Aiello et al., 1977).

$^{40}Ar/^{39}Ar$ analytical techniques

Preparation of the samples before and after irradiation, the $^{40}Ar/^{39}Ar$ analyses, and the age calculations were carried out at the ARGONAUT Laboratory of the Institute for Geology and Palaeontology at the University Salzburg. Mineral concentrates were prepared by crushing, sieving, flotation, and hand-picking of the grain-size of 200–250, respectively 250–355 µm. For measurements 10–20 grains were finally used. Mineral concentrates were packed in aluminium-foil and loaded in quartz vials. For calculation of the J-values, flux-monitors are placed between each 4–5 unknown samples, which yield a distance of ca. 5 mm between adjacent flux-monitors. The sealed quartz vials are irradiated in the MTA KFKI reactor (Debrecen, Hungary) for 16 hours. Correction factors for interfering isotopes have been calculated from 10 analyses of two Ca-glass samples and 22 analyses of two pure K-glass samples, and are: $^{36}Ar/^{37}Ar(Ca) = 0.00026025$, $^{39}Ar/^{37}Ar(Ca) = 0.00065014$, and $^{40}Ar/^{39}Ar(K) = 0.015466$. Variations in the flux of neutrons were monitored with DRA1 sanidine standard for which a $^{40}Ar/^{39}Ar$ plateau age of 25.03 ± 0.05 Ma has been reported (Wijbrans et al., 1995). After irradiation the minerals are unpacked from the quartz vials and the aluminium-foil packets, and handpicked into 1 mm diameter holes within one-way Al-sample holders.

$^{40}Ar/^{39}Ar$ analyses are carried out using a UHV Ar-extraction line equipped with a combined MERCHANTEK™ UV/IR laser ablation facility, and a VG-ISOTECHTM NG3600 Mass Spectrometer.

Stepwise heating analyses of samples are performed using a defocused (~1.5 mm diameter) 25W CO_2-IR laser operating in Tem_{00} mode at wavelengths between 10.57 and 10.63 µm. The laser is controlled from a PC, and the position of the laser within the sample is monitored through a double-vacuum window on the sample chamber

via a video camera in the optical axis of the laser beam on the computer screen. Gas clean-up is performed using one hot and one cold Zr–Al SAES getter. Gas admittance and pumping of the mass spectrometer and the Ar-extraction line are computer controlled using pneumatic valves. The NG3600 is an 18 cm radius 60° extended geometry instrument, equipped with a bright Nier-type source operated at 4.5 kV. Measurement is performed on an axial electron multiplier in static mode, peak-jumping and stability of the magnet is controlled by a Hall-probe. For each increment the intensities of ^{36}Ar, ^{37}Ar, ^{38}Ar, ^{39}Ar, and ^{40}Ar are measured, the baseline readings on mass 35.5 are automatically subtracted. Intensities of the peaks are back-extrapolated over 16 measured intensities to the time of gas admittance either by a straight line or a curved fit. Intensities are corrected for system blanks, background, post-irradiation decay of ^{37}Ar, and interfering isotopes. Isotopic ratios, ages and errors for individual steps are calculated following suggestions by McDougall and Harrison (1999) using decay factors reported by Steiger and Jäger (1977). Definition and calculation of plateau ages has been carried out using ISOPLOT/EX (Ludwig, 2001).

Microfabrics of dated samples

The microfabrics of the dated samples were investigated in detail. A more detailed description of dated samples, including sample locations, is given in the Appendix. We will show and discuss representative samples, which (1) only show monometamorphic (Variscan) high-grade metamorphism without subsequent retrogressive/deformational overprint, and (2) samples with variable overprint by Jurassic respectively Cretaceous retrogressive metamorphism associated with ductile deformation, within lower to upper greenschist facies conditions. Particular attention is given to retrogression of otherwise unaffected basement rocks. In that kind of rocks, retrogression results in pervasive exsolution of opaque, Ti-bearing minerals (e. g. ilmenite) within biotite and phengitic white mica (e. g. Hunziker et al., 1992). This commonly results in a resetting of the Ar isotopic system to younger ages (Hunziker et al., 1992 and references therein).

Migmatitic gneisses (e. g., sample SV-12) show an unretrogressed fabric, characterised by relatively large grains of biotite and muscovite. Biotite does not commonly show exsolution of rutile and other Ti-bearing minerals. This suggests that no later thermal overprint in excess of ca. 300 °C affected these migmatitic paragneisses (Hunziker et al., 1992 and references therein). Amphiboles from unretrogressed amphibolites are optically nearly unzoned.

A specific case is the Poibrene diorite, which shows a well preserved magmatic fabric. The rock shows only minor overprint of secondary alteration. Amphibole grains show some optical zoning and contain round (magmatic) inclusions such as biotite and plagioclase. Biotite grains are round and show some exsolution of ilmenite and occasional chloritisation.

By contrast to unretrogressed basement gneisses, retrogression is dominant in distinct flat-lying shear zones, which increase in number and thickness towards SW. Retrogressed migmatitic gneisses display two white mica generations, exsolution of Ti-bearing minerals from biotite, as well as variable proportions of chloritisation. This retrogression seems to be penetrative in highly sheared mylonitic rocks, for which also Cretaceous ages have been obtained (see below), for example, in sample SV-150. It comprises mica-rich shear zones alternating with fine-grained quartz/plagioclase layers. White mica occurs in ca. 1 mm long fishes showing ilmenite exsolution. Biotite occurs in larger, old flakes with ore exsolution, which are surrounded by new-grown, fine-grained biotite grains. The assemblage of new-grown minerals like albite, sericite, green biotite, clinozoisite and chlorite, indicates lower to possible upper greenschist facies metamorphic conditions.

The small shear zones, observed in retrogressed basement gneisses, increase in width and intensity towards SW, towards the Iskar-Yavoritsa shear zone. They coincide in orientation with ductile shear zones in Upper Carboniferous-Permian cover successions, as exposed around Vakarel (Fig. 2), which include new-grown sericite. There, ductile deformation can be characterised by a flat-lying foliation and an E–W to ESE–WNW trending stretching lineation. Shear sense indicators such as S–C fabrics and porphyroclast systems indicate a dominant top-to-the-W shear.

$^{40}Ar/^{39}Ar$ age dating results

We investigated samples of basement gneiss and ortho-amphibolite from a number of sections within the Central Srednogorie unit, together with one sample of the Poibrene diorite pluton, which displays a clearly discordant contact to the surrounding basement rocks. The $^{40}Ar/^{39}Ar$ dating results of muscovite, biotite, and amphibole are shown in Tables 1–4 and graphically displayed in Figs. 3–6. We first describe samples from basement units, which yield undisturbed Variscan age

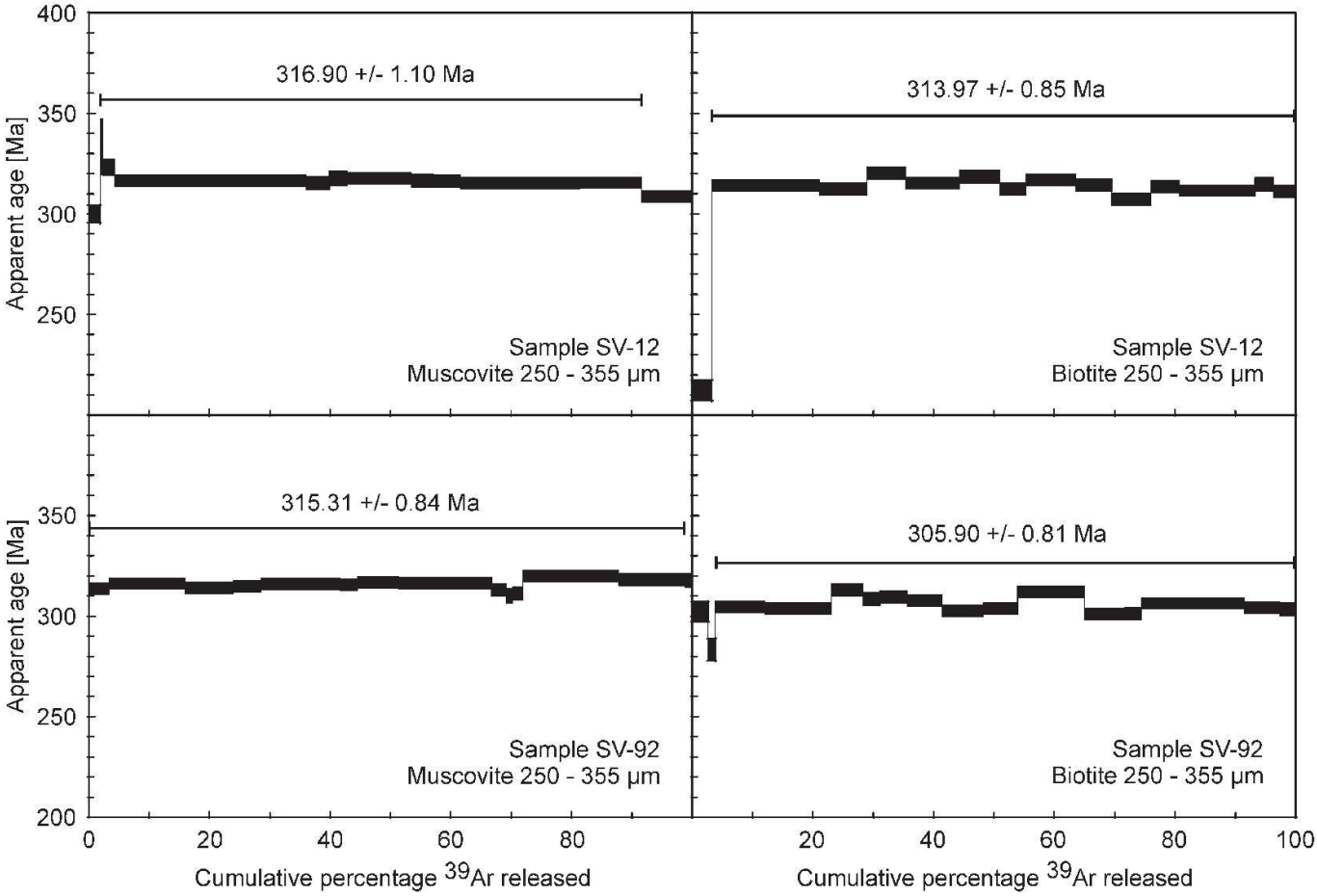

Fig. 3 $^{40}Ar/^{39}Ar$ apparent age spectra with plateau ages of white mica concentrates from the non-retrogressed Srednogorie basement. Laser energy increases from left to right until fusion. Width of the bars represents 1σ error.

patterns (Fig. 3, Table 1), followed by two mineral concentrates from one sample of the Poibrene pluton (Fig. 4, Table 2). Finally, we present analyses from samples, where the Ar-isotopic system has partly (Fig. 5, Table 3) or fully (Fig. 6, Table 4) been reset due to Alpine tectonothermal activity. This approach coincides with the regional distribution, displaying an increase of the metamorphic overprint towards the south.

For the discussion of the geologic significance of our data, estimations for the respective closure temperatures of the Ar-isotopic system in hornblende, muscovite, and biotite are required. Although we know that this topic is under considerable discussion throughout the scientific community (see e.g. Villa, 1998 for a discussion and sug-

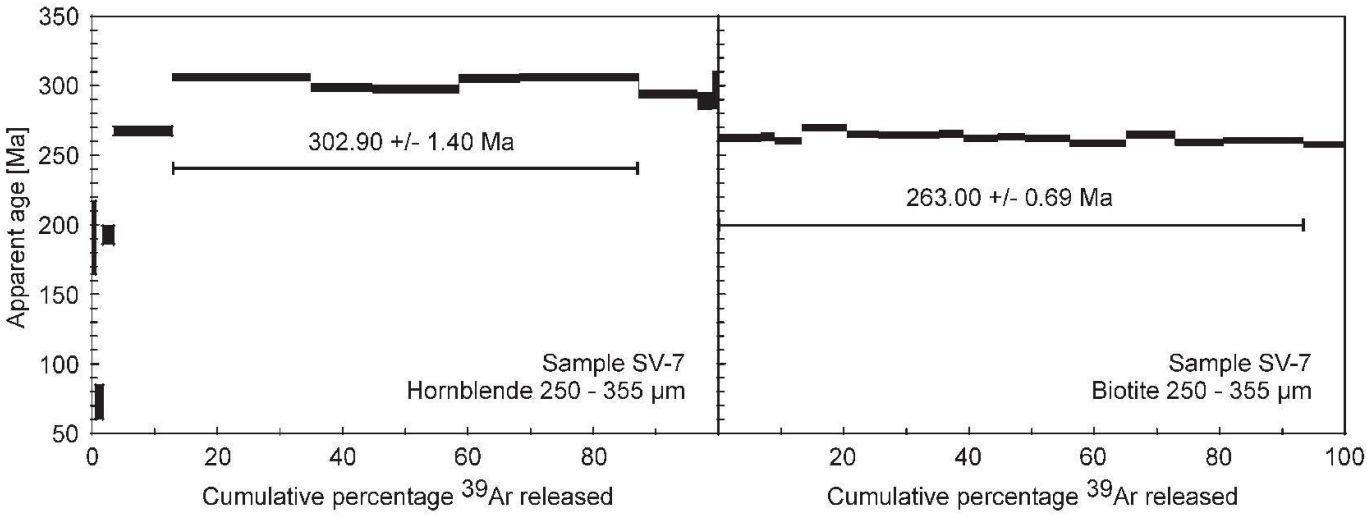

Fig. 4 $^{40}Ar/^{39}Ar$ apparent age spectra with plateau ages of hornblende and biotite concentrates from the Poibrene diorite. Laser energy increases from left to right until fusion. Width of the bars represents 1σ error.

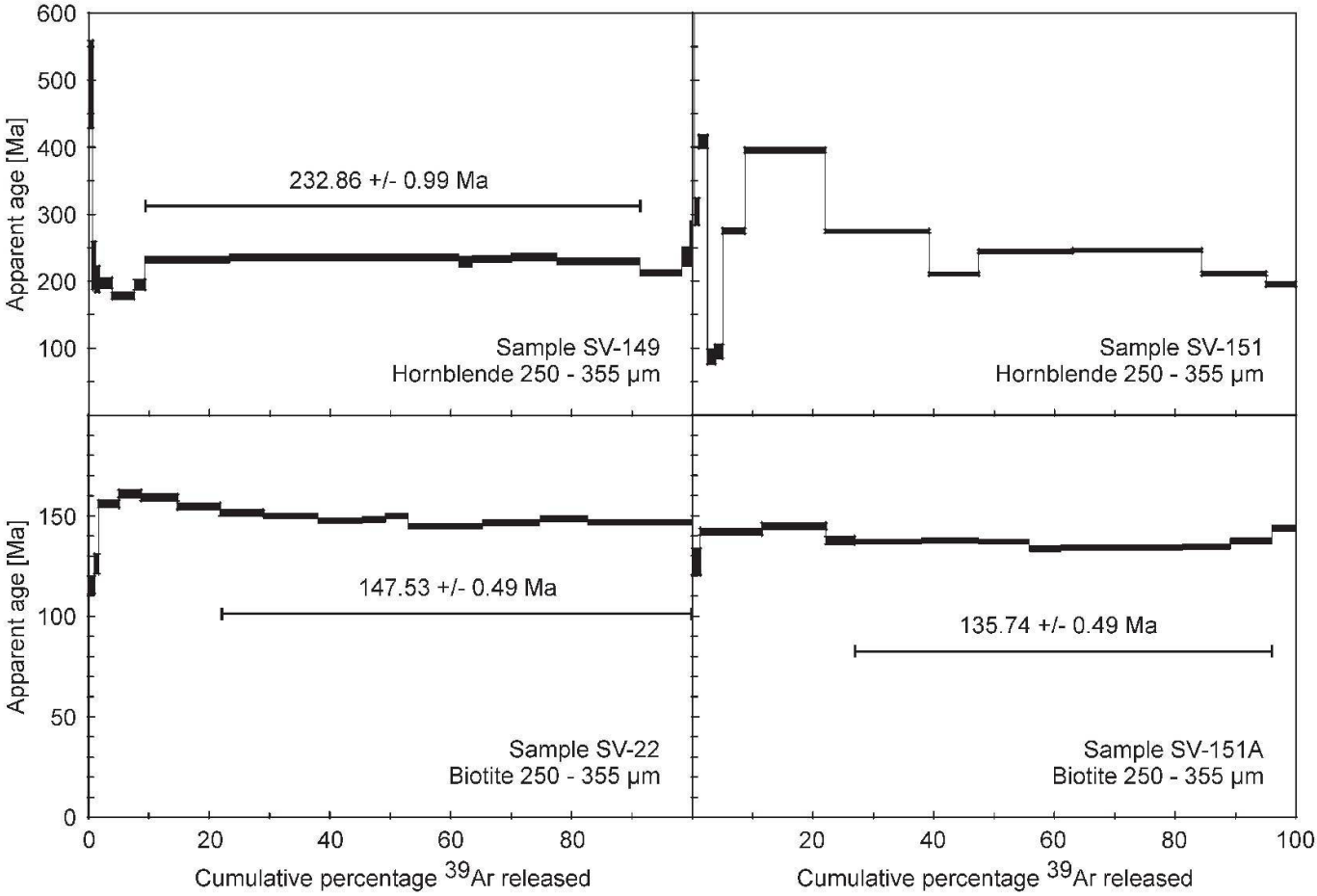

Fig. 5 $^{40}Ar/^{39}Ar$ apparent age spectra of hornblende and biotite concentrates from partly retrogressed gneiss and amphibolite of the Srednogorie basement. Laser energy increases from left to right until fusion. Width of the bars represents 1σ error.

gestions) we decided to refer to closure temperatures for rocks with a single-stage fabric reported earlier in the literature (e.g. von Blanckenburg et al., 1989; Hunziker et al. 1992), which are 500 ± 25 °C for hornblende, 375 ± 25 °C for white mica, and 300 ± 25 °C for biotite.

Variscan basement without later ductile deformation

Two samples of migmatitic, unretrogressed two-mica gneiss without later ductile deformational overprint were collected. SV-12 was sampled 3 km NE of village of Petrich along the Topolnitsa river valley, SV-92 SE of Gol. Rakovitsa. From both samples muscovite and biotite concentrates of the same size-fraction (250–355 µm), which show no exsolution of opaque minerals, have been analysed. The data are reported in Table 1 and graphically presented in Fig. 3. All four concentrates record flat age spectra. Both muscovite concentrates from samples SV-12 and SV-92, and the biotite concentrate from sample SV-12 yielded well defined plateau ages, which are similar within error, and are 316.90 ± 1.10 Ma, 315.31 ± 0.84 Ma, and 313.97 ± 0.85 Ma respectively. Analysis of the biotite concentrate from sample SV-92 again displays an undisturbed distribution of Ar-isotopes, for which a slightly younger plateau age of 305.90 ± 0.81 Ma is reported. Results from both samples are interpreted to be geologically significant and to represent the age of post-metamorphic cooling through respective closure temperatures of the Ar-isotopic system. No radiogenic ^{40}Ar-loss in low-temperature steps is documented. Therefore this excludes Alpine tectonothermal overprint.

Poibrene Diorite

From the Poibrene pluton a diorite sample (SV-7) was collected at the river branch 2 km S of the village of Srebrinovo, from which an amphibole and a biotite concentrate (250–355 µm) was prepared. Data are reported in Table 2 and graphically presented in Fig. 4. Analysis of the amphibole concentrate yielded a stair-case type Ar-release pattern, with ages of ca. 73 Ma, reported in low-energy gas release steps, increasing to a well-defined plateau age of 302.90 ± 1.40 Ma reported for medium- and high-energy gas release steps 5–9 (together comprising 74.5% ^{39}Ar released). A biotite

concentrate from the same sample yielded a completely flat age pattern, recording a plateau age of 263.00 ± 0.69 Ma. Both ages are interpreted to be geologically significant and to represent slow post-magmatic cooling through respective Ar-closure temperatures, e.g. from ca. 500 °C (amphibole) through ca. 300 °C (biotite), corresponding to a cooling rate of ca. 5 °C/Ma.

Partly reset Variscan basement

As mentioned above, the Variscan basement is overprinted by shear zones also caused in retrogression under lower to upper greenschist facies metamorphic conditions. This is also indicated by Ar analyses (Table 3, Fig. 5). Two ortho-amphibolite samples (SV-149 and SV-151) were collected within the Mati Vir River valley. Analyses of hornblende concentrates yielded contrasting age spectra for both samples: For sample SV-149 a flat argon release spectrum yielding a plateau age of 232.86 ± 0.99 Ma. However, low-energy gas release steps reveal both incorporation and loss of ^{40}Ar components, which implies a disturbance of the Ar-isotopic signature after initial isotopic closure. The other hornblende, sample SV-151, yielded a completely disturbed age pattern, with ages ranging from ca. 400 Ma to ca. 90 Ma in low-energy gas release steps, and ages of ca. 250–200 Ma in medium- and high-energy gas release steps. No plateau is defined for this sample.

Two biotite-gneiss samples were collected, one 1.5 km ESE of village of Vakarel (SV-22), and one from the Mati Vir River valley (SV-151A). For both samples plateau ages are reported. Biotite from sample SV-22 displays a complex age pattern within the first six low-energy gas release steps (together comprising 29.0% ^{39}Ar released). Within the first four gas release steps ages increasing from ca. 110 Ma to ca. 160 Ma, then ages continuously decrease to define a plateau (steps 9–17: 71.0% ^{39}Ar released) recording an age of 147.53 ± 0.49 Ma. This pattern is not monitored by the ^{37}Ar/^{39}Ar ratio (Table 3), and therefore cannot be explained by a probable existence of different mineralogical phases with different Ca/K ratios evolving gas throughout the heating experiment, and therefore would be responsible for this age pattern. We therefore conclude that the Ar-release pattern of biotite sample SV-22 indicates incorporation of excess ^{40}Ar components, probably throughout the age spectrum, which could not be resolved by the step-wise heating technique. Ar analysis of biotite from sample SV-151A reveals an obviously flat age pattern with a plateau age of 135.74 ± 0.49 Ma. Although not as well resolved as the pattern previously described, the same general trend of Ar-release pattern is indicated.

Together, the ages reported for the four samples are not entirely clear. They could be interpreted to be geologically meaningless, and to be due to incorporation and/or loss of ^{40}Ar components, due to a tectonothermal overprint subsequent to initial isotopic closure. However, we tentatively interpret these ages therefore as a weak indication of a low-grade metamorphic/tectonothermal event, which occurred at ca. the Jurassic-Cretaceous boundary.

Fully reset Variscan basement

A number of basement gneisses show mylonitic fabrics, which are the result of a low-grade, but pervasive tectonometamorphic overprint. From these lithologies three samples were collected within the Mati Vir River valley, from two of these samples muscovite and biotite concentrates were prepared. The data are reported in Table 4 and graphically presented in Fig. 6.

A muscovite concentrate from a basement gneiss SV-149A yielded a nearly completely flat gas release-spectrum with an age of 105.35 ± 0.35 Ma. From another gneiss sample (SV-150) muscovite and biotite have been separated. Low-energy gas release steps obtained for the muscovite are significantly higher than the reported plateau age of 102.22 ± 0.55 Ma, which would argue for incorporation of excess ^{40}Ar components, similar as reported for biotite from sample SV-22 (see above). However, by contrast to the SV-22 biotite age spectrum, the fluctuation in ages reported for muscovite concentrate of sample SV-150, is monitored by the ^{37}Ar/^{39}Ar ratios (Table 4), which are significantly higher for the first five gas release steps compared to steps 6–11 (together comprising 78.5% ^{39}Ar released), which are used to define the plateau. It is therefore concluded, that an optically undetectable, less retentive, mineralogically different phase with a higher Ca-content contributed gas through the first five gas release steps of the experiment. A biotite concentrate from the same sample yielded a fairly flat plateau with an age of 103.56 ± 0.36 Ma. Muscovite and biotite concentrates prepared from sample SV-150A yielded flat gas release patterns, beside some minor fluctuations in the low-energy gas release steps and plateaus, recording the same age within error of 99.57 ± 0.31 Ma (muscovite) and 99.55 ± 0.36 Ma (biotite) respectively.

Taken together, the plateau ages, ranging between 106–100 Ma, reported for five concentrates from three samples of mylonitic gneiss samples are interpreted to be geologically significant. Be-

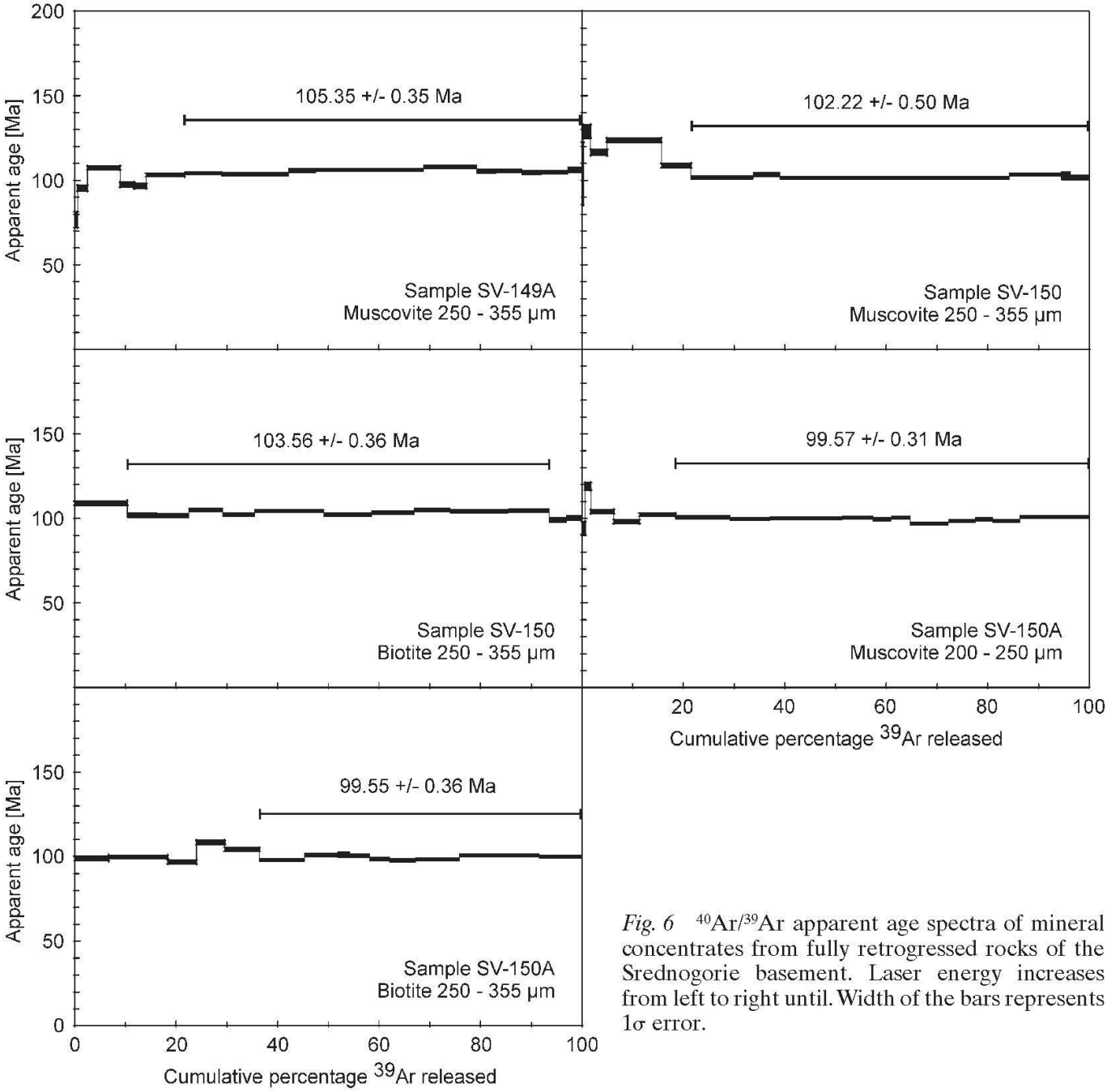

Fig. 6 $^{40}Ar/^{39}Ar$ apparent age spectra of mineral concentrates from fully retrogressed rocks of the Srednogorie basement. Laser energy increases from left to right until. Width of the bars represents 1σ error.

cause ages reported for new grown biotite and muscovite are mutually similar within error, ages are interpreted to actually date the time of ductile deformation under lower greenschist facies metamorphic conditions, at ca. 350–450 °C, close to the estimated closure temperatures for the Ar-isotopic system in muscovite (Hunziker et al., 1992; Villa, 1998; McDougall and Harrison, 1999).

Discussion

The new $^{40}Ar/^{39}Ar$ mineral ages from Srednogorie basement constrain a number of tectonic events. These include the age of post-metamorphic cooling of the basement and its retrogressive overprint through possibly three tectonic events. These are similar to recent data reported in a conference abstract by Mukasa et al. (2003). The closure of the Ar isotopic system of minerals, like white mica, biotite and amphibole, depends on many factors, including maximum metamorphic temperature, duration of heating, deformation, chemical composition of minerals and hydrothermal fluids, among other factors (e. g. Villa, 1998). In regional metamorphic and plutonic basement rocks, which are not affected by secondary processes, the classical closure temperatures can be applied as a reasonable estimate, keeping in mind all limitations of that approach.

The age of post-metamorphic cooling through ca. 375 ± 25 °C subsequent to high-grade, partly migmatite-grade, metamorphism in unretrogressed Variscan basement is ca. 317–315 Ma (musco-

vite ages). Cooling through 300 ± 25 °C is recorded by biotite ages and took place between 314 and 306 Ma. These ages are widespread and similar to those found in the Southern and Western Carpathians and in the Apuseni Mountains (Dallmeyer et al., 1996, 1998), in the lateral extension of the Srednogorie unit (Fig. 1a). This seems to constrain that the Balkanide-type basement may be part of a major piece of continental crust, which has a characteristic lithological composition and Variscan age for, e. g., the Getic and Supragetic nappe complexes in the Southern Carpathians, although all authors correlated these units with the Serbomacedonian unit, which is exposed further to the west (Fig. 1a,b; Sandulescu, 1984; Kräutner, 1993; Dimitrijevic, 1997; Haydoutov et al., 1997; Karamata et al., 1997). The ages also suggest that the last amphibolite-grade metamorphic overprint occurred during late Variscan orogenic events. This links the Srednogorie basement through the Alpine-Carpathian basement with the Central-Western European Variscides (Matte, 1991; von Raumer, 1998).

The basement has been intruded by a number of plutons after high-grade metamorphism, possibly during waning stages of cooling and after exhumation from deep to middle crustal levels. The amphibole age from the Poibrene diorite is in accordance with other data, including high-precision U–Pb zircon ages of the same pluton and other post-Variscan plutons of the Srednogorie unit (Arnaudov et al., 1989; Kamenov et al., 2002; Carrigan et al., 2003).

The biotite plateau age of 263.0 ± 0.69 Ma from the Poibrene diorite indicates that Permian cooling affected the intrusions within the basement. Whether these ages indicate a widespread tectonothermal event or one of only local importance, mainly affecting the Poibrene diorite, is uncertain. However, regional comparison shows that such events are similar in age to those in the whole ABCD region (e. g. Dallmeyer et al., 1996, 1998), and most likely indicating a similar process of crustal extension or a heat pulse due to heating in lower levels of the lithosphere.

A few data argue for a possible weak thermal overprint at the Jurassic-Cretaceous boundary. The Late Jurassic age group is consistent with tectonic events of the same age, which has been recorded in the Sakar-Strandja zone representing the southeastern extension of the Srednogorie unit (Dimitrov, 1956, 1958; Chatalov, 1990; Ivanov et al., 2001a; Okay et al., 2001), in the southernmost Moesian platform (Tari et al., 1997) and in the South Carpathian orogen (Bojar et al., 1998). Consequently, these ages are not isolated and could represent a widespread tectonic event. However, more data are needed to confirm this idea.

A number of muscovite and biotite ages from mylonitic basement gneisses indicates that the southern parts of the Central Srednogorie basement was overprinted by pervasive Alpine metamorphism associated with ductile deformation between 106 and 100 Ma. This event seems to be of short duration and reached temperatures typical for upper greenschist facies metamorphic conditions.

Previous data show that the retrogressed basement was intruded by late-stage plutons, which clearly postdate, according to their fabric and field relationships, the age of a 106–100 Ma tectonic event. The ages of these granitoids range between 84 and 78 Ma (e. g. von Quadt et al., 2002; Kamnov et al., 2002; Peytcheva and von Quadt, 2003; Handler et al., 2004). The southernmost of these granitoids intruded at depths corresponding to pressures of 4–6 kbar (Ivanov et al., 2002; Georgiev and Lazarova, 2003). As the northernmost granitoids and basement rocks are unmetamorphic, these relationships suggest a northward, late Cretaceous tilting and exhumation of southernmost granitoids. Exhumation occurred within a transtensive setting as some of these granitoids were ductilely deformed under solid-stage conditions within the NW-trending dextral Iskar-Yavoritsa shear zone.

Conclusions

Our new $^{40}Ar/^{39}Ar$ mineral data give evidence for the following major conclusions:

(1) The age of the last high-grade metamorphic overprint in the Srednogorie unit is Late Variscan. Therefore, we correlate the Balkanide-type basement with the Getic/Supragetic nappe complexes of South Carpathians.

(2) There is some evidence for possible Permian and Late Jurassic tectonothermal events in the Srednogorie basement, which need support by further detailed studies.

(3) The timing of the Alpine ductile overprint is between 106 and 100 Ma. This event predates the formation of the volcanosedimentary Srednogorie basin and related Banatite intrusions.

Acknowledgements

We acknowledge discussions with many colleagues, including Albrecht von Quadt, Irena Peytcheva and Neven Georgiev. Careful reviews by Clark Burchfiel and Stefan Schmid and suggestions by Thomas Driesner helped to clarify data presentation and ideas. We grate-

fully acknowledge support by the GEODE Grants for Visit Programme, which made this study possible. Final work has been supported by grant P15.646-GEO of the Austrian Research Foundation (FWF) to FN. SV and ZI gratefully acknowledge the support of Sofia University Scientific Research Foundation. Final work has been also supported by grant no. 7BUPJ62396 of the Swiss Research Foundation (SNF, SCOPES) to SV.

References

Aiello, E., Bartolini, C., Bocaletti, M., Gocev, P., Karagjuleva, J., Kostadinov, V. and Manetti, P. (1977): Sedimentary features of the Srednogorie zone (Bulgaria), an Upper Cretaceous intra-arc basin. *Sed. Geol.* **19**, 39–68.

Arnaudov, V., Amov, B., Bratnitzkii, B. and Pavlova, M. (1989): Isotopic geochronology of magmatic and metamorphic rocks from Balkanides and Rhodope massif. XIV – Congress of CBGA, Sofia, Sept. 1989, 1154–1157. (In Russian).

Barr, S.R., Temperley, S. and Tarney, J. (1999): Lateral growth of the continental crust trough deep level subduction-accretion: arc-evaluation of central Greek Rhodope. *Lithos* **46**, 69–94.

Berza, T., Constantinescu, E. and Vlad, S.N. (1998): Upper Cretaceous magmatic series and associated mineralisation in the Carpathian-Balkan Orogen. *Resource Geol.* **48**, 291–306.

Blanckenburg, F.V., Villa, I.M., Baur, H., Morteani, G. and Steiger. R.H. (1989): Time calibration of a PT-path from the Western Tauern Window, Eastern Alps: The problem of closure temperatures. *Contrib. Mineral. Petrol.* **101**, 1–11.

Bocaletti, M., Manetti, P. and Peccerillo, A. (1974): The Balkanids as an instance of back-arc thrust belt: Possible relation with the Hellenides. *Geol. Soc. Am. Bull.* **85**, 1077–1084.

Bocaletti, M., Manetti, P., Peccerillo, A. and Stanisheva-Vasilieva, G. (1978): The Late Cretaceous high-potassium volcanism in eastern Srednogorie, Bulgaria. *Geol. Soc. Am. Bull.* **89**, 439–447.

Bojar, A.V., Neubauer, F. and Fritz, H. (1998): Cretaceous to Cenozoic thermal evolution of the southwestern South Carpathians: evidence from fission-track thermochronology. *Tectonophysics* **297**, 229–249.

Burchfiel, B.C. (1980): Eastern European alpine system and the Carpathian orocline as an example of collision tectonics. *Tectonophysics* **63**, 31–61.

Burg, J.P., Ivanov, Z., Ricou, L.E., Dimor, D. and Klain, L. (1990): Implication of shear-sense criteria for the tectonic evolution of the Central Rhodope massif, southern Bulgaria. *Geology* **18**, 451–454.

Burg, J.P., Ricou, L., Ivanov, Z., Godfriaux, I., Dimov, D. and Klain, L. (1993): Crustal-scale thrust complex in the Rhodope massif. Structure and Kinematics. *Bull. Geol. Soc. Greece* **XXVIII**, 71–85.

Carrigan, C.W., Mukasa, S.B., Haydoutov, I. and Kolcheva, K. (2003): Ion microprobe U–Pb zircon ages of pre-Alpine rocks in the Balkan, Sredna Gora, and Rhodope Terranes of Bulgaria: Constraints on Neoproterozoic and Variscan tectonic evolution. *J. Czech Geol. Soc.* **48**, 32.

Chatalov, G. (1990). Geology of Srandza zone in Bulgaria. Publishing House of the Bulg. Acad. of Sci., Sofia. 256 pp.

Channell, J.E.T. and Kozur, H. (1997): How many oceans? Meliata, Vardar, and Pindos oceans in Mesozoic Alpine paleogeography. *Geology* **25**, 183–186.

Dallmeyer, R.D., Neubauer, F., Handler, R., Fritz, H., Müller, W., Pana, D. and Putis, M. (1996): Tectonothermal evolution of the internal Alps and Carpathians: Evidence from $^{40}Ar/^{39}Ar$ mineral and whole rock data. *Ecl. geol. Helv.* **89**, 203–227.

Dallmeyer, R.D., Neubauer, F., Fritz, H. and Mocanu, V. (1998): Variscan vs. Alpine tectonothermal evolution of the South Carpathian orogen: constraints from $^{40}Ar/^{39}Ar$ ages. *Tectonophysics* **290**, 111–135.

Dimitrijevic, M.D. (1997): Geology of Yugoslavia. Geological Institute GEMINI, Belgrade, 187 pp.

Dimitrov, S. (1956): Die kinetische Regionalmetarmorphose der jurassischen Ablagerungen und Leukogranite in Südostbulgarien. Abh. 20, Intern. Geologenkongr., Mexico. In: *Akad. Str. Dimitrov, Wiss. Werke* **2**, 333–342.

Dimitrov, S. (1958): Über die alpidische Regionalmetamorphose und ihre Beziehungen zu der Tektonik und dem Magmatismus in Südostbulgarien. *Geologie* **7**, 560–568.

Dimitrov, Str. (1959): Kurze Übersicht der metamorphen Komplexe in Bulgarien. *Freiburger Forschungshefte* **C 57**, 62–72.

Dimitrova, E. and Belmustakova, H. (1982): Metamorphic facies of the crystalline schists complex of Ihtiman Sredna Gora Mountains. *Geochem. Mineral. Petrol.*, **16**, 61–67. (In Bulgarian with English and German abstracts).

Foose, R.M. and Manheim, F. (1975): Geology of Bulgaria. *Am. Assoc. Petrol. Geol. Bull.* **59**, 303–335.

Georgiev, N. and Lazarova, A. (2003): Magma mixing in Upper Cretaceous plutonic bodies in the southwestern parts of the Central Sredna gora zone, Bulgaria. *C. R. Bulg. Acad. Sci.* **56**, 4, 47–52.

Handler, R., Velichkova, S.H., Neubauer, F. and Ivanov, Z. (2004): $^{40}Ar/^{39}Ar$ age constraints on the timing of magmatism and post-magmatic cooling in the Panagyurishte region, Bulgaria. *Schweiz. Mineral. Petrogr. Mitt.* **84**, 119–132.

Haydoutov, I. and Yanev, S. (1997): The Protomoesian microcontinent of the Balkan Peninsula – a peri-Gondwanaland piece. *Tectonophysics* **272**, 303–313.

Haydoutov, I., Gochev, P., Kozhoukhraov, D. and Yaney, S. (1997): Terranes in the Balkan area. In: Papanikolao, D. (ed.): IGCP project no. 276 Terrane map and terrane descriptions. *Annales Géologiques des Pays Helléniques* **37** (1996–97), 479–494.

Heinrich, C.A. and Neubauer, F. (2002): Cu-Au(-Pb-Zn-Ag) metallogeny of the Alpine-Balkan-Carpathian-Dinaride geodynamic province: introduction. *Min. Deposita* **37**, 533–540.

Hsü, K., Nachev, I. and Vuchev, V. (1977): Geological evolution of Bulgaria in light of plate tectonics. *Tectonophysics* **40**, 245–256.

Hunziker, J.C., Desmons, J. and Hurford, A.J. (1992): Thirty-two years of geochronological work in the Central and Western Alps: a review of seven maps. *Mem. Geol. Lausanne* **13**, 1–59.

Ivanov, Z. (1983): Apercu general sur l'evolution geologique et structurale des Balkanides. In: Ivanov, Z. and Nikolov, T. (eds.): Guide de l'excursion. Reunion Extraordinaire de la Societé geologique de France en Bulgarie. *Soc. Geol. Bulg. Press University*, Sofia, pp. 3–26.

Ivanov, Z. (1988): Apercu general sur l'evolution geologique et structurale du massif des Rhodopes dans le card des Balkanides. *Bull. Soc. Geol. France* **8**, 227–240.

Ivanov, Z. (1989a): Structure and tectonic evolution of central parts of the Rhodope massif. In: Ivanov, Z. (ed.): Structure and Geodynamic Evolution of the

inner zones of Balkanides – Kraishtides and Rhodope Area. Guide for excursion XIV Congress CBGA, Sofia, Bulgaria, pp. 56–92.

Ivanov, Z. (ed.). (1989b): Structure and tectonic evolution of the central parts of the Rhodope massif. In: Giude to excursion E-3, CBGA – XIV Congress, S., Bulgaria, 126 pp.

Ivanov, Z., Moskovski, S. and Kolcheva, K. (1979): Basic features of the Structure of the Central Parts of the Rhodope massif. *Geologica Balcanica* **9**, 1, 30–50. (In Russian, abstract in English).

Ivanov, Z., Gerdjikov, I. and Kounov, A. (2001a): New data and consideration about structure and tectonic evolution of Sakar region, Southeast Bulgaria. *Ann. de L'Univ. de Sofia "ST. Kliment Ohridski", Fac. de Geol. Geogr. Geol.* **91**, 35–80.

Ivanov, Z., Henry, B., Dimov, D. Georgiev, N., Jordanova, D. and Jordanova, N. (2001b): New model for Upper Cretaceous magma emplacement in the southwestern parts of Central Srednogorie – petrostructural and AMS data. *Rom. J. Mineral Deposits* **79**, Suppl. 2, 60–61.

Ivanov, Z., Georgiev, N. Lazarova, A. and Dimov, D. (2002): New model of upper Cretaceous magma emplacement in the southwestern parts of Central Sredna Gora zone, Bulgaria. *Geologica Carpathica* **53**, spec issue, Proc. the XVII. Congress of CBGA, Bratislava (CD version).

Kamenov, B., von Quadt, A. and Peytcheva, I. (2002): New insight into petrology, geochemistry and dating of the Vejen pluton, Bulgaria. *Geochem. Mineral. Petrol.* **39**, 3–25

Karagjuleva, J., Kostadinov, V., Tzankov, Tz. and Gocev, P. (1974): Structure of the Panagjuriste strip east of the Topolnitsa river. *Bull. Geol. Inst., ser. Geotectonics* **13**, 231–301.

Karamata, S., Krstic, B., Dimitrijevic, D.M., Dimitrijevic, M.N., Kneevic, V., Stojanov, R. and Filipovic, I. (1997): Terranes between the Moesian plate and the Adriatic Sea. In: Papanikolao, D. (ed.): IGCP project no. 276 Terrane map and terrane descriptions. *Annales Géologiques des Pays Helléniques* **37** (1996–97), 429–477.

Kozhukharov, D., Kozhukharova, E. and Zagorchev, I. (1978): The Precambrian in Bulgaria. In: Precambrian in young fold belts. IGCP Project 22, 65 pp.

Kräutner, H.G. (1993): Pre-Alpine evolution in the Southern Carpathians and adjacent areas. *Geologica Carpathica* **44**, 203–212.

Krohe, A. and Mposkos, E. (2002): Multiple generations of extensional detachments in the Rhodope Mountains (northern Greece): evidence of episodic exhumation of high-pressure rocks. In: Blundell, D.J., Neubauer, F. and von Quadt, A. (eds.): The timing and location of major ore deposits in an evolving orogen. *Geol. Soc. (London) Spec. Publ.* **204**, 151–178.

Liu, Y., Genser, J., Handler, R., Friedl, G. and Neubauer, F. (2001): $^{40}Ar/^{39}Ar$ muscovite ages from the Penninic/Austroalpine plate boundary, eastern Alps. *Tectonics* **20**, 528–547.

Ludwig, K.R. (2001): Isoplot/Ex – A Geochronological Toolkit for Microsoft Excel. *Berkeley Geochronological Center Special Publication No.* 1a.

Matte, P. (1991): Accretionary history and crustal evolution of the Variscan belt in Western Europe. *Tectonophysics* **196**, 309–337.

McDougall, I. and Harrison, M.T. (1999): Geochronology and thermochronology by the $^{40}Ar/^{39}Ar$ method. 2nd Ed, Oxford University Press, Oxford, 269 pp.

Minkovska, V., Peybernès, B., Nikolov, T. and Ivanov, M. (2002): Paleogeographic reconstruction of a segment of the North-Tethyan margin in Bulgaria from Barremian to Albian. *Ecl. geol. Helv.* **95**, 183–195.

Mukasa, S.B., Haydoutov, I., Carrigan, C.W. and Kolcheva, K. (2003): Thermobarometry and $^{40}Ar/^{39}Ar$ ages of eclogitic and gneissic rocks in the Sredna Gora and Rhodope Terranes of Bulgaria. *J. Czech Geol. Soc.* **48**, 94.

Nachev, I.K. (1993): Late Cretaceous palaeogeodynamics of Bulgaria. *Geologica Balcanica* **23**, 3–23.

Neubauer, F. (2002a): Contrasting Late Cretaceous to Neogene ore provinces in the Alpine-Balkan-Carpathian-Dinaride collision belt. In: Blundell, D.J., Neubauer, F. and von Quadt, A. (eds.): The timing and location of major ore deposits in an evolving orogen. *Geol. Soc. (London) Spec. Publ.* **204**, 81–102.

Neubauer, F. (2002b): Evolution of late Neoproterozoic to early Paleozoic tectonic elements in central and southeast European Alpine mountain belts: review and synthesis. *Tectonophysics* **352**, 87–103.

Neubauer, F., Dallmeyer, R.D., Dunkl, I. and Schirnik, D. (1995): Late Cretaceous exhumation of the metamorphic Gleinalm dome, Eastern Alps: kinematics, cooling history and sedimentary response in a sinistral wrench corridor. *Tectonophysics* **242**, 79–89.

Neugebauer, J., Greiner, B. and Appel, E. (2001): Kinematics of Alpine-West Carphian orogen and palaeogeographic implications. *J. Geol Soc. (London)* **158**, 97–110.

Okay, A. I., Satir, M., Tüysüz, O., Akyüz, S. and Chen, F. (2001): The tectonics of the Strandja Massif: late Variscan and mid-Mesozoic deformation and metamorphism in the northern Aegean. *Int. J. Earth Sci.* **90**, 217–233.

Peytcheva, I. and von Quadt, A. (2003): U–Pb-zircon isotope system in mingled and mixed magmas: an example from Central Srednogorie, Bulgaria. *Geophysical Research Abstracts* 5, 09177, Nice, (electronic version).

Popov, P. and Popov, K. (2000): General geologic and metallogenic features of the Panagyrishte ore region. In: Strashimirov, S. and Popov, P. (eds.): Geology and metallogeny of the Panagyurishte ore region (Srednogorie zone, Bulgaria). *Guide to Excursions A and C. ABCD-GEODE 2000 Workshop, Borovets Bulgaria,* p. 1–7.

Quadt, A. von, Peycheva, I., Kamenov, B., Fanger, L. and Heinrich, C.A. (2002): The Elatitse porphyry copper deposit of the Panagyurishte ore district, Srednogorie unit, Bulgaria: U–Pb zircon geochronology and isotope-geochemical investigations of ore genesis. In: Blundell, D., Neubauer, F. and von Quadt, A. (eds.): The timing and location of major ore deposits in an evolving orogen. *Geol. Soc. Spec. Publ. (London)* **204**, 119–135.

Raumer, J. von (1998): The Paleozoic evolution in the Alps: from Gondwana to Pangea. *Geol. Rundschau* **87**, 407–435.

Ricou, L.E., Burg, J.P., Godfriaux, I. and Ivanov, Z. (1998): Rhodope and Vardar: the metamorphic and the olistostromic paired belts related to the Cretaceous subduction under Europe. *Geodinamica Acta* **11**, 285–309.

Royden, L.H. (1988): Late Cenozoic tectonics of the Pannonian basin system. *Am. Assoc. Petrol. Geol. Mem.* **45**, 27–48.

Sandulescu, M. (1984): Geotectonica Romaniei. Ed. Tehnica, Bucharest, 336 pp.

Stampfli, C.M. and Mosar, J. (1999): The making and becoming of Apulia. *Mem. Sci. Geol.* **51**, 141–154.

Steiger, R.H. and Jäger, E. (1977): Subcommission on geochronology: Convention on the use of decay con-

stants in geo-and cosmochronology. *Earth Planet. Sci. Lett.* **36**, 359–362
Tari, G., Dicea, O., Faulkerson, J., Georgiev, G., Popov, S., Stenaescu, M. and Weir, G. (1997): Cimmerian and Alpine stratigraphy and structural evolution of the Moesian Platform (Romania/Bulgaria). In: Robinson, A.G. (ed.): Regional and petroleum geology of the Black Sea and surrounding region. *Am. Assoc. Petr. Geol. Mem.* **68**, 63–90.
Villa, I. (1998): Isotopic closure. *Terra Nova* **10**, 42–47.
Wijbrans, J.R., Pringle, M.S., Koopers, A.A.P. and Schveers, R. (1995): Argon geochronology of small samples using the Vulkaan argon laserprobe. *Proc. Kon. Ned. Akad. Wetensch.* **98**, 185–218.
Willingshofer, E., Neubauer, F. and Cloetingh, S. (1999): Significance of Gosau basins for the upper Cretaceous geodynamic history of the Alpine-Carpathian belt. *Phys. Chem. Earth Part A: Solid Earth Geodesy* **24**, 687–695.
Zagorcev, I. (1993): Multiphase crustal thickening in the central parts of the Balkan Peninsula. *Bull. Geol. Soc. Greece* **XXIX**, 87–97.

Received 24 October 2003
Accepted in revised form 8 August 2004
Editorial handling: T. Driesner

Appendix

Petrographic characteristics of dated rocks

Samples are described in the same order as they appear in the text.

Sample SV-12: Location: 3 km NE of Petrich along the Tolponitsa River valley. Two-mica gneiss of the unretrogressed basement. The gneiss comprises a well-preserved metamorphic fabric. It includes brown biotite grains, only a few of them with subordinate exsolution of opaque minerals and chlorite. White mica occurs in two generations: Large (1 mm long) mica flakes contain many euhedral inclusions, and are partly recrystallised to smaller white mica grains.

Sample SV-92 is from SE edge of Gol. Rakovitsa. Coarse-grained two-mica gneiss. The gneiss comprises 0.5–3 mm large mica grains; 0.6 mm large garnet grains are partly chloritised along margins. Quartz is well annealed and displays some amoeboid boundaries due to grain boundary migration.

Sample SV-7: Location is from a roadcut from Petrich to Poibrene, 2 km S of the branch to Srebrinovo. Biotite-hornblende diorite. Well preserved magmatic fabric with plagioclase, brownish amphibole, biotite and some quartz as main constituents, and magmatic epidote, zircon, ore minerals, apatite as minor constituents. Plagioclase is optically zoned and sometimes transformed to clinozoisite in core zones and patchy sericite at rims. Amphibole shows some optical zoning and bears round (magmatic) inclusions as biotite and plagioclase. Biotite grains are round and show some exsolution of platy opaque minerals (ilmenite), respectively sometimes transformation to chlorite.

Sample SV-22: Roadcut 1.5 km ESE of Vakarel. Mylonitic gneiss with S–C-fabric respectively a porphyroclastic fabric with σ-type alkali feldspar and plagioclase porphyroclasts. Biotite is 0.2–0.3 mm in size, greenish and intergrown with chlorite. White mica grains occur as fishes and are surrounded by fine sericite (ca. 0.2 mm). Quartz occurs in small elongated grains. Further minerals are sphene, rutile and opaque minerals.

Sample SV-151: Mati Vir. Amphibolite with a well-preserved, statically annealed fabric and minerals, which are ca. 0.4–0.5 mm in diameter. Amphibole is optically unzoned and contains few inclusions (ca. 0.05 mm in size) of quartz and plagioclase. Plagioclase comprises patches with transformation into fine sericite, starting along cracks. Biotite is sometimes marginally transformed to chlorite. Further minerals are sphene, opaque minerals, apatite and zircon.

Sample SV-149: Mati Vir River valley. Amphibolite with a static, annealed fabric. The grain size is ca. 0.5 to 1.5 mm. Amphibole is optically unzoned and contains small round inclusions of plagioclase, quartz, epidote and apatite.

Sample SV-150: Mati Vir river valley. Sheared two-mica gneiss. Narrow mica-rich shear zones alternate with quartz/plagioclase layers. White micas comprise ca. 1 mm long fishes and show ilmenite exsolution. Biotite occurs in larger, old flakes with ore exsolution, which are surrounded by fine-grained biotite grains. Chlorite, opaque minerals, sphene, apatite and zircon are further, rare minerals.

Sample 150A: Same locality as SV-150. Mati Vir river valley. Biotite gneiss. Biotite and white mica form layers with recrystallised grains, which are 0.2–0.5 mm in length. Biotite shows retrogression with ore mineral exsolution. Greenish biotite locally occurs. Plagioclase includes some small garnet inclusions, respectively is altered to a fine-grained mixture of phyllosilicates.

Table 1 Ar-analytical data from laser-step-heating experiments on muscovite and biotite multi-grain samples from basement rocks of the Panagyuriste region, Bulgaria.

Sample: SV-12 Muscovite (250–355 µm)
J-Value: 0.02223 +/– 0.00022

step	$^{36}Ar/^{39}Ar^a$	+/–	$^{37}Ar/^{39}Ar^b$	+/–	$^{40}Ar/^{39}Ar^a$	+/–	$\%^{40}Ar^c$	$\%^{39}Ar$	age [Ma]	+/–
1	0.00862	0.00034	0.00601	0.00028	10.69742	0.09972	76.2	1.9	299.92	4.37
2	0.00101	0.00137	0.00304	0.00116	9.44645	0.40706	96.9	0.5	333.50	13.91
3	0.00250	0.00028	0.00363	0.00024	9.57993	0.08440	92.3	2.0	323.21	4.09
4	0.00067	0.00002	0.00032	0.00001	8.83686	0.00611	97.7	31.7	316.36	2.91
5	0.00075	0.00015	0.00213	0.00013	8.82634	0.04454	97.5	3.9	315.28	3.26
6	0.00177	0.00021	0.00011	0.00024	9.19787	0.06335	94.3	3.0	317.64	3.61
7	0.00070	0.00006	0.00041	0.00006	8.88373	0.01844	97.7	10.6	317.65	2.98
8	0.00084	0.00015	0.00292	0.00016	8.89070	0.04499	97.2	3.7	316.51	3.27
9	0.00147	0.00014	0.00267	0.00013	9.07511	0.04020	95.2	4.4	316.44	3.20
10	0.00063	0.00003	0.00051	0.00003	8.79413	0.00848	97.9	19.8	315.34	2.91
11	0.00074	0.00006	0.00171	0.00006	8.83029	0.01885	97.5	10.2	315.53	2.96
12	0.00095	0.00007	0.00129	0.00007	8.69015	0.02032	96.8	8.5	308.67	2.92
steps 2–11								89.7	316.90	1.10

Sample: SV-12 Biotite (250–355 µm)
J-Value: 0.02214 +/– 0.00022

step	$^{36}Ar/^{39}Ar^a$	+/–	$^{37}Ar/^{39}Ar^b$	+/–	$^{40}Ar/^{39}Ar^a$	+/–	$\%^{40}Ar^c$	$\%^{39}Ar$	age [Ma]	+/–
1	0.12456	0.00044	0.00905	0.00017	42.45991	0.13035	13.3	3.2	212.15	5.04
2	0.02892	0.00007	0.00350	0.00003	17.15092	0.02024	50.2	17.9	314.15	2.96
3	0.01065	0.00011	0.00177	0.00007	11.69605	0.03387	73.1	7.8	312.19	3.08
4	0.00116	0.00010	0.00268	0.00009	9.13208	0.03049	96.3	6.4	320.29	3.10
5	0.00092	0.00007	0.00152	0.00008	8.91719	0.02155	96.9	8.9	315.41	2.98
6	0.00207	0.00011	0.00325	0.00009	9.34897	0.03318	93.4	6.7	318.48	3.12
7	0.00267	0.00014	0.00608	0.00013	9.34360	0.04259	91.6	4.4	312.42	3.20
8	0.00132	0.00007	0.00843	0.00007	9.07541	0.02095	95.7	8.3	316.80	2.98
9	0.00208	0.00011	0.00857	0.00012	9.22511	0.03303	93.3	5.9	314.30	3.09
10	0.00186	0.00009	0.00907	0.00008	8.94866	0.02695	93.9	6.5	307.21	2.96
11	0.00005	0.00012	0.00828	0.00015	8.60539	0.03460	99.8	4.7	313.60	3.10
12	0.00044	0.00005	0.00749	0.00005	8.65859	0.01608	98.5	12.6	311.53	2.91
13	0.00035	0.00020	0.00543	0.00019	8.72324	0.05955	98.8	3.1	314.63	3.51
14	0.00043	0.00015	0.00075	0.00015	8.64659	0.04404	98.5	3.6	311.20	3.21
steps 2–14								96.8	313.97	0.85

Sample: SV-92 Muscovite (250–355 µm)
J-Value: 0.02205 +/– 0.00022

step	$^{36}Ar/^{39}Ar^a$	+/–	$^{37}Ar/^{39}Ar^b$	+/–	$^{40}Ar/^{39}Ar^a$	+/–	$\%^{40}Ar^c$	$\%^{39}Ar$	age [Ma]	+/–
1	0.00547	0.00010	0.00150	0.00009	10.24652	0.02863	84.2	3.4	313.73	3.03
2	0.00163	0.00003	0.00061	0.00002	9.18549	0.00876	94.7	12.6	316.18	2.91
3	0.00096	0.00004	0.00001	0.00004	8.92362	0.01121	96.8	8.0	314.04	2.90
4	0.00058	0.00007	0.00087	0.00007	8.83328	0.02118	98.0	4.6	314.77	2.97
5	0.00050	0.00002	0.00069	0.00002	8.84518	0.00668	98.3	13.1	315.98	2.90
6	0.00132	0.00011	0.00174	0.00009	9.07395	0.03141	95.7	3.0	315.58	3.07
7	0.00108	0.00005	0.00005	0.00005	9.04318	0.01466	96.5	6.8	316.86	2.94
8	0.00036	0.00002	0.00039	0.00002	8.82151	0.00616	98.8	15.4	316.58	2.90
9	0.00264	0.00011	0.00268	0.00011	9.38616	0.03154	91.7	2.5	312.93	3.05
10	0.00216	0.00023	0.00535	0.00025	9.15739	0.06962	93.0	1.1	310.04	3.68
11	0.00334	0.00018	0.00539	0.00016	9.54107	0.05440	89.7	1.7	311.21	3.38
12	0.00073	0.00002	0.00041	0.00002	9.02594	0.00585	97.6	15.9	319.76	2.93
13	0.00013	0.00003	0.00005	0.00003	8.79955	0.00896	99.6	10.9	318.17	2.93
14	0.00000	0.00019	0.00031	0.00021	8.75167	0.05572	100.0	1.3	317.77	3.45
steps 1–13								98.7	315.31	0.84

Errors of ratios, J-values, and ages are at 1-sigma level. continued
a) measured
b) corrected for post-irradiation decay of ^{37}Ar (35.1 days)
c) non atmospheric ^{40}Ar

Table 1 continued.

Sample: SV-92 Biotite (250–355 μm)
J-Value: 0.02196 +/– 0.00022

step	$^{36}Ar/^{39}Ar^a$	+/–	$^{37}Ar/^{39}Ar^b$	+/–	$^{40}Ar/^{39}Ar^a$	+/–	$\%^{40}Ar^c$	$\%^{39}Ar$	age [Ma]	+/–
1	0.13725	0.00040	0.00419	0.00020	48.87931	0.12405	17.0	2.6	302.26	5.00
2	0.01511	0.00048	0.01178	0.00045	12.22238	0.14211	63.5	1.2	283.26	5.48
3	0.00554	0.00009	0.00152	0.00007	10.03514	0.02598	83.7	8.3	304.79	2.94
4	0.00522	0.00007	0.00035	0.00005	9.91049	0.02125	84.4	10.9	303.79	2.89
5	0.00111	0.00010	0.00057	0.00012	8.96809	0.02965	96.3	5.3	312.93	3.04
6	0.00061	0.00018	0.00887	0.00021	8.68963	0.05392	97.9	2.8	308.56	3.36
7	0.00139	0.00012	0.00847	0.00012	8.94907	0.03425	95.4	4.6	309.50	3.07
8	0.00166	0.00010	0.00643	0.00010	8.96947	0.02936	94.5	5.7	307.57	3.00
9	0.00212	0.00009	0.00624	0.00009	8.96054	0.02711	93.0	6.9	302.71	2.94
10	0.00087	0.00011	0.00511	0.00009	8.62643	0.03258	97.0	5.7	303.92	3.01
11	0.00103	0.00005	0.00073	0.00005	8.92120	0.01356	96.6	11.1	312.15	2.91
12	0.00091	0.00009	0.00038	0.00009	8.55818	0.02544	96.9	6.7	301.18	2.91
13	0.00122	0.00018	0.00244	0.00025	8.64803	0.05340	95.8	2.7	301.18	3.31
14	0.00062	0.00003	0.00043	0.00004	8.63053	0.00912	97.9	17.0	306.43	2.84
15	0.00021	0.00009	0.00044	0.00011	8.44397	0.02546	99.3	6.0	304.25	2.93
16	0.00027	0.00019	0.00394	0.00025	8.43527	0.05613	99.1	2.6	303.43	3.37
steps 3–16								96.2	305.90	0.81

Errors of ratios, J-values, and ages are at 1-sigma level.
a) measured
b) corrected for post-irradiation decay of ^{37}Ar (35.1 days)
c) non atmospheric ^{40}Ar

Table 2 Ar-analytical data from laser-step-heating experiments on hornblende, and biotite multi-grain samples from the Poibrene pluton of the Panagyuriste region, Bulgaria.

Sample: SV-7 Hornblende (250–355 μm)
J-Value: 0.02187 +/– 0.00022

step	$^{36}Ar/^{39}Ar^a$	+/–	$^{37}Ar/^{39}Ar^b$	+/–	$^{40}Ar/^{39}Ar^a$	+/–	$\%^{40}Ar^c$	$\%^{39}Ar$	age [Ma]	+/–
1	0.10961	0.00240	6.78114	0.00397	36.96138	0.73070	12.4	0.6	190.81	26.00
2	0.05088	0.00107	4.12354	0.00181	16.60785	0.31811	9.5	1.1	72.66	12.08
3	0.01826	0.00059	12.40159	0.00278	9.56841	0.17468	43.6	1.8	192.65	6.46
4	0.00894	0.00019	10.58452	0.00051	9.10149	0.05551	71.0	9.3	267.54	3.12
5	0.00656	0.00008	15.10043	0.00040	9.16981	0.02489	78.9	22.1	306.28	2.94
6	0.00655	0.00016	15.68382	0.00065	8.89543	0.04765	78.3	9.9	298.77	3.18
7	0.00697	0.00013	15.17819	0.00052	9.02828	0.03924	77.2	13.8	297.61	3.04
8	0.00604	0.00016	13.10855	0.00061	9.14657	0.04639	80.5	9.7	305.15	3.20
9	0.00628	0.00011	14.95679	0.00046	9.09845	0.03212	79.6	19.0	306.26	3.01
10	0.00538	0.00020	11.77710	0.00065	8.73191	0.05822	81.8	9.4	294.08	3.34
11	0.00782	0.00060	14.23770	0.00208	9.10642	0.17735	74.6	2.4	289.18	6.53
12	0.00846	0.00134	13.52339	0.00432	9.58708	0.39852	73.9	1.0	297.08	13.61
steps 5–9								74.5	302.90	1.40

Sample: SV-7 Biotite (250–355 μm)
J-Value: 0.02200 +/– 0.00022

step	$^{36}Ar/^{39}Ar^a$	+/–	$^{37}Ar/^{39}Ar^b$	+/–	$^{40}Ar/^{39}Ar^a$	+/–	$\%^{40}Ar^c$	$\%^{39}Ar$	age [Ma]	+/–
1	0.08074	0.00012	0.01188	0.00006	30.99499	0.03610	23.0	6.8	262.57	2.74
2	0.00622	0.00018	0.01260	0.00018	9.00053	0.05302	79.6	2.2	263.49	3.05
3	0.02366	0.00012	0.00675	0.00008	14.06611	0.03581	50.3	4.3	260.43	2.72
4	0.00455	0.00007	0.00330	0.00004	8.69462	0.02012	84.5	7.2	269.91	2.60
5	0.00263	0.00008	0.00401	0.00007	7.98871	0.02339	90.3	5.1	265.17	2.59
6	0.00503	0.00005	0.00468	0.00004	8.68056	0.01429	82.9	9.7	264.52	2.51
7	0.00199	0.00009	0.00411	0.00009	7.81138	0.02727	92.5	3.9	265.50	2.64
8	0.00194	0.00006	0.00767	0.00005	7.70561	0.01937	92.6	5.4	262.42	2.53
9	0.00083	0.00006	0.00705	0.00007	7.39694	0.01776	96.7	4.4	263.11	2.52
10	0.00049	0.00005	0.01064	0.00005	7.27246	0.01429	98.0	7.2	262.26	2.49
11	0.00044	0.00003	0.01106	0.00003	7.15017	0.00954	98.2	9.0	258.57	2.43
12	0.00047	0.00004	0.00983	0.00005	7.34208	0.01101	98.1	7.8	264.91	2.49
13	0.00082	0.00005	0.01074	0.00005	7.28631	0.01496	96.7	7.8	259.39	2.47
14	0.00030	0.00002	0.01073	0.00003	7.17138	0.00703	98.8	12.7	260.76	2.44
15	0.00040	0.00004	0.01896	0.00004	7.11353	0.01294	98.3	6.6	257.72	2.44
steps 1–14								93.4	263.00	0.69

Table 3 Ar-analytical data from laser-step-heating experiments on hornblende and biotite multi-grain samples from partly resetted basement rocks of the Panagyuriste region, Bulgaria.

Sample: SV-149 Hornblende (250–355 μm)
J-Value: 0.02187 +/– 0.00022

step	$^{36}Ar/^{39}Ar^{a}$	+/–	$^{37}Ar/^{39}Ar^{b}$	+/–	$^{40}Ar/^{39}Ar^{a}$	+/–	$\%^{40}Ar^{c}$	$\%^{39}Ar$	age [Ma]	+/–
1	0.10675	0.00139	2.80722	0.00153	45.70771	0.41614	31.0	0.6	493.66	13.21
2	0.02674	0.00153	1.23199	0.00204	13.84914	0.45449	43.0	0.4	223.59	15.98
3	0.01364	0.00090	1.98666	0.00153	9.33173	0.26556	56.8	0.7	203.02	9.56
4	0.00861	0.00035	5.24006	0.00086	7.41708	0.10321	65.7	2.1	197.06	4.10
5	0.00601	0.00019	6.98778	0.00063	5.98295	0.05610	70.3	3.7	178.29	2.63
6	0.00584	0.00033	7.30072	0.00100	6.37731	0.09821	72.9	1.8	195.07	3.94
7	0.00375	0.00006	9.62218	0.00023	6.63129	0.01684	83.3	14.0	232.39	2.26
8	0.00338	0.00002	9.25204	0.00011	6.63723	0.00682	85.0	37.8	235.41	2.22
9	0.00341	0.00030	8.89067	0.00077	6.48410	0.08824	84.5	2.2	228.75	3.74
10	0.00402	0.00010	8.97820	0.00042	6.78079	0.03066	82.5	6.5	232.99	2.43
11	0.00350	0.00009	9.95004	0.00042	6.62815	0.02560	84.4	7.5	235.80	2.38
12	0.00327	0.00006	10.08636	0.00022	6.36839	0.01646	84.8	13.7	229.54	2.23
13	0.00323	0.00010	8.33284	0.00040	6.00839	0.02877	84.1	6.8	212.32	2.24
14	0.00457	0.00059	9.40922	0.00136	7.00934	0.17341	80.7	1.3	236.52	6.40
15	0.00572	0.00130	10.10545	0.00302	7.85126	0.38479	78.5	0.5	255.90	13.39
steps 7–12								81.7	232.86	0.99

Sample: SV-151 Hornblende (250–355 μm)
J-Value: 0.02201 +/– 0.00022

step	$^{36}Ar/^{39}Ar^{a}$	+/–	$^{37}Ar/^{39}Ar^{b}$	+/–	$^{40}Ar/^{39}Ar^{a}$	+/–	$\%^{40}Ar^{c}$	$\%^{39}Ar$	age [Ma]	+/–
1	0.07607	0.00367	0.82061	0.00399	65.92124	1.14273	65.9	0.4	1211.93	24.80
2	0.02993	0.00198	0.43078	0.00240	17.16793	0.58989	48.5	0.7	304.11	19.99
3	0.03663	0.00095	0.49423	0.00102	22.33300	0.28450	51.5	1.5	408.16	9.72
4	0.01342	0.00098	0.65368	0.00123	6.18661	0.28854	35.9	1.2	87.46	10.95
5	0.01042	0.00090	1.25993	0.00142	5.45214	0.26570	43.5	1.3	95.00	10.05
6	0.00944	0.00029	4.25959	0.00071	9.93456	0.08718	71.9	3.6	274.92	3.92
7	0.00488	0.00012	7.77716	0.00031	11.94517	0.03508	87.9	13.3	395.64	3.72
8	0.00311	0.00008	6.67386	0.00025	7.85459	0.02475	88.3	17.2	274.46	2.68
9	0.00391	0.00015	7.74631	0.00052	6.17822	0.04529	81.3	8.2	210.77	2.55
10	0.00398	0.00009	7.47623	0.00035	7.17735	0.02680	83.6	15.6	244.41	2.47
11	0.00371	0.00006	8.24300	0.00028	7.09035	0.01905	84.6	21.4	246.42	2.40
12	0.00316	0.00015	7.84742	0.00045	5.95890	0.04406	84.3	10.7	211.16	2.53
13	0.00309	0.00030	6.46945	0.00087	5.61521	0.08912	83.8	4.9	195.75	3.68
14	0.05017	0.02119	77.31480	0.14884	63.51505	6.48359	76.7	0.1	1475.66	114.07
no plateau										

Sample: SV-22 Biotite (250–355 μm)
J-Value: 0.02222 +/– 0.00022

step	$^{36}Ar/^{39}Ar^{a}$	+/–	$^{37}Ar/^{39}Ar^{b}$	+/–	$^{40}Ar/^{39}Ar^{a}$	+/–	$\%^{40}Ar^{c}$	$\%^{39}Ar$	age [Ma]	+/–
1	1.06249	0.00740	0.17796	0.00243	316.52375	2.78294	0.8	0.1	99.70	105.57
2	0.05490	0.00038	0.01952	0.00023	19.21434	0.11254	15.6	1.0	115.60	4.37
3	0.01609	0.00042	0.02175	0.00028	8.02549	0.12564	40.8	0.7	126.09	4.85
4	0.00685	0.00010	0.00888	0.00007	6.10242	0.02940	66.8	3.4	155.97	1.83
5	0.00330	0.00008	0.00249	0.00007	5.19281	0.02320	81.2	3.6	161.03	1.75
6	0.00426	0.00005	0.00247	0.00004	5.42138	0.01612	76.8	6.0	159.07	1.62
7	0.00067	0.00003	0.00432	0.00004	4.24417	0.01011	95.4	7.0	154.80	1.52
8	0.00053	0.00004	0.00377	0.00004	4.11306	0.01183	96.2	7.2	151.45	1.50
9	0.00091	0.00003	0.00415	0.00003	4.18701	0.00976	93.6	9.1	150.02	1.47
10	0.00087	0.00004	0.00374	0.00003	4.11040	0.01149	93.7	7.3	147.62	1.47
11	0.00022	0.00007	0.00272	0.00006	3.93409	0.02048	98.4	3.9	148.25	1.60
12	0.00031	0.00007	0.00315	0.00007	4.00649	0.02110	97.7	3.7	149.97	1.62
13	0.00043	0.00002	0.00673	0.00002	3.89899	0.00736	96.7	12.4	144.63	1.40
14	0.00023	0.00003	0.00507	0.00003	3.88920	0.00865	98.3	9.5	146.49	1.43
15	0.00014	0.00003	0.00742	0.00003	3.91977	0.00976	98.9	7.9	148.57	1.46
16	0.00032	0.00002	0.02088	0.00004	3.91763	0.00722	97.6	8.9	146.63	1.42
17	0.00032	0.00002	0.06227	0.00004	3.91679	0.00727	97.6	8.4	146.64	1.42
steps 9–17								71.0	147.53	0.49

Table 3 continued.

Sample: SV-151A Biotite (250–355 μm)
J-Value: 0.02241 +/–0.00022

step	$^{36}Ar/^{39}Ar^a$	+/–	$^{37}Ar/^{39}Ar^b$	+/–	$^{40}Ar/^{39}Ar^a$	+/–	$\%^{40}Ar^c$	$\%^{39}Ar$	age [Ma]	+/–
1	0.20688	0.00054	0.00764	0.00026	64.40452	0.17062	5.1	1.3	127.13	6.55
2	0.04864	0.00008	0.00336	0.00003	18.04417	0.02389	20.4	10.2	142.11	1.63
3	0.00732	0.00005	0.00278	0.00004	5.90711	0.01585	63.4	10.6	144.83	1.51
4	0.01024	0.00012	0.00203	0.00006	6.58394	0.03631	54.0	4.8	137.78	1.90
5	0.00566	0.00004	0.00386	0.00003	5.21233	0.01150	67.9	11.1	137.10	1.39
6	0.00273	0.00004	0.00604	0.00004	4.36067	0.01062	81.5	9.4	137.68	1.38
7	0.00391	0.00004	0.00640	0.00004	4.69428	0.01129	75.4	8.4	137.09	1.39
8	0.00390	0.00006	0.01443	0.00003	4.59695	0.01918	74.9	5.2	133.60	1.48
9	0.00410	0.00005	0.01078	0.00005	4.66961	0.01589	74.0	5.7	134.08	1.42
10	0.00273	0.00003	0.00693	0.00002	4.26543	0.00797	81.1	14.5	134.16	1.33
11	0.00181	0.00003	0.00952	0.00004	4.01141	0.00994	86.6	8.0	134.75	1.35
12	0.00111	0.00005	0.00677	0.00006	3.87608	0.01441	91.5	6.9	137.47	1.43
13	0.00059	0.00007	0.00841	0.00009	3.89293	0.02106	95.5	3.9	143.83	1.59
steps 5–12								69.2	135.74	0.49

Errors of ratios, J-values, and ages are at 1-sigma level.
a) measured
b) corrected for post-irradiation decay of ^{37}Ar (35.1 days)
c) non atmospheric ^{40}Ar

Table 4 Ar-analytical data from laser-step-heating experiments on muscovite and biotite multi-grain samples from completely resetted basement rocks of the Panagyuriste region, Bulgaria.

Sample: SV-149A Muscovite (250–355 μm)
J-Value: 0.02209 +/– 0.00022

step	$^{36}Ar/^{39}Ar^a$	+/–	$^{37}Ar/^{39}Ar^b$	+/–	$^{40}Ar/^{39}Ar^a$	+/–	$\%^{40}Ar^c$	$\%^{39}Ar$	age [Ma]	+/–
1	0.00795	0.00041	0.00719	0.00049	4.32946	0.12003	45.7	0.6	76.63	4.65
2	0.00397	0.00014	0.00196	0.00013	3.64331	0.04084	67.8	2.0	95.29	1.80
3	0.00055	0.00004	0.00176	0.00004	2.95470	0.01043	94.5	6.4	107.35	1.11
4	0.00189	0.00009	0.00349	0.00009	3.08272	0.02725	81.9	2.8	97.37	1.40
5	0.00138	0.00011	0.00082	0.00014	2.91098	0.03225	86.0	2.3	96.57	1.54
6	0.00065	0.00004	0.00086	0.00004	2.87069	0.01054	93.3	7.6	103.09	1.07
7	0.00071	0.00004	0.00107	0.00004	2.91149	0.01126	92.8	7.4	103.97	1.09
8	0.00032	0.00002	0.00079	0.00002	2.78331	0.00632	96.6	13.1	103.55	1.03
9	0.00013	0.00005	0.00058	0.00006	2.78606	0.01500	98.6	5.4	105.72	1.17
10	0.00052	0.00003	0.00060	0.00003	2.90974	0.00932	94.7	10.3	106.05	1.08
11	0.00018	0.00003	0.00100	0.00003	2.80761	0.00789	98.1	11.0	105.95	1.07
12	0.00013	0.00003	0.00006	0.00003	2.84349	0.00956	98.6	10.5	107.86	1.10
13	0.00002	0.00008	0.00003	0.00008	2.73702	0.02389	99.8	3.7	105.15	1.36
14	0.00002	0.00006	0.00049	0.00006	2.74827	0.01758	99.7	5.1	105.47	1.22
15	0.00056	0.00008	0.00393	0.00008	2.88048	0.02370	94.3	3.8	104.53	1.35
16	0.00033	0.00005	0.00159	0.00006	2.81938	0.01611	96.5	5.2	104.74	1.18
17	0.00069	0.00011	0.00121	0.00011	2.96279	0.03182	93.1	2.8	106.13	1.58
steps 7–17								78.4	105.35	0.35

Sample: SV-150 Muscovite (250–355 μm)
J-Value: 0.02193 +/– 0.00022

step	$^{36}Ar/^{39}Ar^a$	+/–	$^{37}Ar/^{39}Ar^b$	+/–	$^{40}Ar/^{39}Ar^a$	+/–	$\%^{40}Ar^c$	$\%^{39}Ar$	age [Ma]	+/–
1	0.01179	0.00167	0.02570	0.00139	6.20182	0.49450	43.8	0.3	103.96	18.50
2	0.01134	0.00035	0.01115	0.00028	6.74251	0.10481	50.3	1.4	128.87	4.06
3	0.00193	0.00014	0.00410	0.00013	3.62488	0.04162	84.3	3.2	116.46	1.91
4	0.00078	0.00005	0.00140	0.00004	3.48248	0.01334	93.4	10.8	123.73	1.29
5	0.00084	0.00008	0.00360	0.00007	3.08844	0.02279	92.0	5.8	108.49	1.35
6	0.00072	0.00003	0.00004	0.00003	2.87240	0.00907	92.5	12.2	101.64	1.04
7	0.00132	0.00007	0.00075	0.00007	3.09244	0.02177	87.4	5.3	103.33	1.29
8	0.00048	0.00001	0.00026	0.00001	2.79034	0.00209	95.0	45.2	101.32	0.99
9	0.00068	0.00004	0.00009	0.00004	2.90632	0.01154	93.1	10.3	103.42	1.09
10	0.00116	0.00021	0.00065	0.00022	3.03145	0.06180	88.7	1.8	102.80	2.52
11	0.00067	0.00009	0.00127	0.00013	2.85472	0.02703	93.1	3.6	101.62	1.41
steps 6–11								78.5	102.22	0.50

Table 4 continued.

Sample: SV-150 Biotite (250–355 μm)
J-Value: 0.02185 +/– 0.00022

step	$^{36}Ar/^{39}Ar^a$	+/–	$^{37}Ar/^{39}Ar^b$	+/–	$^{40}Ar/^{39}Ar^a$	+/–	$\%^{40}Ar^c$	$\%^{39}Ar$	age [Ma]	+/–
1	0.01508	0.00007	0.00187	0.00004	7.32302	0.02184	39.2	10.4	109.08	1.33
2	0.00800	0.00009	0.00008	0.00008	5.04316	0.02801	53.1	5.8	102.09	1.44
3	0.00292	0.00007	0.00168	0.00008	3.53121	0.02134	75.5	6.3	101.61	1.27
4	0.00221	0.00005	0.00365	0.00007	3.41362	0.01493	80.9	6.7	105.11	1.16
5	0.00165	0.00005	0.00570	0.00006	3.17270	0.01358	84.7	6.3	102.33	1.12
6	0.00107	0.00003	0.00209	0.00003	3.05983	0.00897	89.6	13.6	104.41	1.07
7	0.00091	0.00004	0.00329	0.00004	2.95251	0.01102	90.9	9.4	102.22	1.08
8	0.00035	0.00005	0.00152	0.00006	2.81826	0.01427	96.3	8.4	103.34	1.14
9	0.00054	0.00005	0.00075	0.00007	2.91511	0.01561	94.5	7.1	104.87	1.17
10	0.00042	0.00003	0.00137	0.00004	2.86327	0.00995	95.7	11.6	104.29	1.08
11	0.00020	0.00005	0.00001	0.00005	2.80426	0.01357	97.9	8.0	104.54	1.13
12	0.00027	0.00012	0.00484	0.00012	2.67792	0.03435	97.0	3.4	99.07	1.60
13	0.00027	0.00013	0.00041	0.00016	2.71194	0.03704	97.1	3.0	100.30	1.69
steps 2–11								83.2	103.56	0.36

Sample: SV-150A Muscovite (200–250 μm)
J-Value: 0.02233 +/– 0.00022

step	$^{36}Ar/^{39}Ar^a$	+/–	$^{37}Ar/^{39}Ar^b$	+/–	$^{40}Ar/^{39}Ar^a$	+/–	$\%^{40}Ar^c$	$\%^{39}Ar$	age [Ma]	+/–
1	0.00916	0.00031	0.00623	0.00032	5.12795	0.09144	47.2	0.6	94.47	3.61
2	0.00305	0.00017	0.00264	0.00020	3.97019	0.05088	77.3	1.1	118.98	2.23
3	0.00094	0.00004	0.00067	0.00005	2.95095	0.01137	90.6	4.5	104.05	1.09
4	0.00143	0.00004	0.00123	0.00003	2.93788	0.01181	85.7	5.0	98.04	1.04
5	0.00080	0.00003	0.00066	0.00003	2.85970	0.00783	91.7	7.1	102.10	1.02
6	0.00088	0.00002	0.00086	0.00002	2.84629	0.00659	90.9	10.7	100.71	1.00
7	0.00046	0.00002	0.00041	0.00002	2.69846	0.00625	95.0	7.9	99.83	0.99
8	0.00065	0.00001	0.00044	0.00001	2.76165	0.00430	93.0	14.2	100.04	0.97
9	0.00051	0.00003	0.00019	0.00003	2.73610	0.00860	94.5	6.1	100.68	1.02
10	0.00037	0.00005	0.00025	0.00005	2.66411	0.01597	95.8	3.6	99.46	1.13
11	0.00023	0.00004	0.00010	0.00006	2.65186	0.01206	97.4	3.8	100.56	1.07
12	0.00022	0.00003	0.00040	0.00003	2.55458	0.00759	97.4	7.5	97.01	0.97
13	0.00002	0.00003	0.00027	0.00004	2.52855	0.00956	99.8	5.4	98.31	1.01
14	0.00001	0.00005	0.00055	0.00006	2.55377	0.01433	99.9	3.4	99.36	1.10
15	0.00005	0.00003	0.00104	0.00004	2.54083	0.00988	99.4	5.4	98.36	1.02
16	0.00008	0.00001	0.00004	0.00001	2.61726	0.00322	99.1	13.6	101.02	0.98
steps 6–16								81.5	99.57	0.31

Sample: SV-150A Biotite (250–355 μm)
J-Value: 0.02217 +/– 0.00022

step	$^{36}Ar/^{39}Ar^a$	+/–	$^{37}Ar/^{39}Ar^b$	+/–	$^{40}Ar/^{39}Ar^a$	+/–	$\%^{40}Ar^c$	$\%^{39}Ar$	age [Ma]	+/–
1	0.02349	0.00010	0.00177	0.00005	9.50160	0.02859	27.0	6.7	99.07	1.45
2	0.00371	0.00004	0.00080	0.00003	3.68113	0.01043	70.2	11.6	99.90	1.05
3	0.00064	0.00006	0.00121	0.00006	2.69421	0.01766	93.0	5.6	96.93	1.16
4	0.00008	0.00007	0.00025	0.00006	2.83087	0.02016	99.2	5.6	108.33	1.30
5	0.00044	0.00005	0.00077	0.00005	2.82739	0.01539	95.4	6.8	104.16	1.17
6	0.00047	0.00003	0.00077	0.00003	2.67185	0.00991	94.8	8.9	98.00	1.03
7	0.00026	0.00005	0.00106	0.00005	2.68712	0.01487	97.1	6.5	100.92	1.13
8	0.00034	0.00013	0.00070	0.00014	2.71984	0.03821	96.3	2.4	101.29	1.75
9	0.00019	0.00006	0.00217	0.00008	2.65462	0.01893	97.8	3.9	100.43	1.21
10	0.00033	0.00007	0.00229	0.00008	2.64775	0.01950	96.3	3.9	98.64	1.21
11	0.00034	0.00006	0.00186	0.00006	2.63188	0.01664	96.2	5.0	97.95	1.14
12	0.00035	0.00003	0.00200	0.00003	2.64293	0.01010	96.1	8.7	98.24	1.03
13	0.00022	0.00003	0.00107	0.00003	2.66695	0.00805	97.6	10.3	100.63	1.03
14	0.00024	0.00006	0.00151	0.00006	2.67750	0.01677	97.4	5.4	100.81	1.17
15	0.00016	0.00003	0.00142	0.00004	2.63091	0.00968	98.2	8.5	99.94	1.04
steps 6–15								63.6	99.55	0.36

Errors of ratios, J-values, and ages are at 1-sigma level.
a) measured
b) corrected for post-irradiation decay of ^{37}Ar (35.1 days)
c) non atmospheric ^{40}Ar